Neuron

Article

# Ketamine exerts its sustained antidepressant effects via cell-type-specific regulation of *Kcnq2*

## Graphical abstract

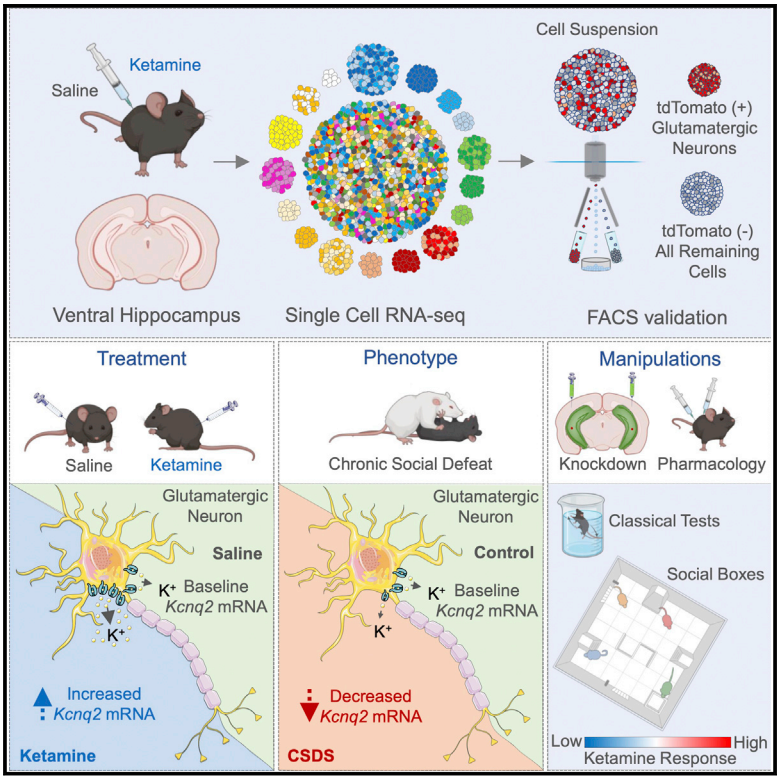


## Highlights

- scRNA-seq reveals cell-type-specific molecular signatures of ketamine treatment
- The *Kcnq2* gene is identified as an important modulator of ketamine action
- Adjunctive treatment with retigabine augments ketamine's antidepressant effects
- A novel mechanism underlying the sustained antidepressant effects of ketamine


## Authors

Juan Pablo Lopez, Malte D. Lücken, Elena Brivio, ..., Julien Dine, Fabian J. Theis, Alon Chen

## Correspondence

alon.chen@weizmann.ac.il



## In brief

Lopez et al. identify cell-type-specific changes associated with the sustained antidepressant effects of ketamine. They demonstrate that the combined treatment of ketamine with a KCNQ activator leads to stronger effects. Their findings provide a deeper understanding of the complex mechanisms underlying the antidepressant effects of ketamine, with important clinical implications.


Lopez et al., 2022, Neuron *110*, 2283–2298
July 20, 2022 
https://doi.org/10.1016/j.neuron.2022.05.001

CellPress

Neuron

CellPress

Article

# Ketamine exerts its sustained antidepressant effects via cell-type-specific regulation of *Kcnq2*

Juan Pablo Lopez,[1] Malte D. Lücken,[2] Elena Brivio,[1] Stoyo Karamihalev,[1] Aron Kos,[1] Carlo De Donno,[1,2] Asaf Benjamin,[3,4] Huanqing Yang,[1] Alec L.W. Dick,[1] Rainer Stoffel,[1] Cornelia Flachskamm,[1] Andrea Ressle,[1] Simone Roeh,[5] Rosa-Eva Huettl,[1] Andrea Parl,[1] Carola Eggert,[1] Bozidar Novak,[6] Yu Yan,[6] Karin Yeoh,[6] Maria Holzapfel,[1] Barbara Hauger,[1] Daniela Harbich,[1] Bianca Schmid,[1] Rossella Di Giaimo,[7] Christoph W. Turck,[6] Mathias V. Schmidt,[1] Jan M. Deussing,[1] Matthias Eder,[1] Julien Dine,[1,3] Fabian J. Theis,[2] and Alon Chen[1,3,4,8,*]

[1]Department of Stress Neurobiology and Neurogenetics, Max Planck Institute of Psychiatry, Munich, 80804 Bavaria, Germany
[2]Institute of Computational Biology, Helmholtz Zentrum München, German Research Center for Environmental Health, Neuherberg, 85764 Bavaria, Germany
[3]Department of Brain Sciences, Weizmann Institute of Science, Rehovot 76100, Israel
[4]Department of Molecular Neuroscience, Weizmann Institute of Science, Rehovot 76100, Israel
[5]Department of Translational Research in Psychiatry, Max Planck Institute of Psychiatry, Munich, 80804 Bavaria, Germany
[6]Proteomics and Biomarkers, Max Planck Institute of Psychiatry, Munich, 80804 Bavaria, Germany
[7]Department of Developmental Neurobiology, Max Planck Institute of Psychiatry, Munich, 80804 Bavaria, Germany
[8]Lead contact
*Correspondence: alon.chen@weizmann.ac.il
https://doi.org/10.1016/j.neuron.2022.05.001

## SUMMARY

A single sub-anesthetic dose of ketamine produces a rapid and sustained antidepressant response, yet the molecular mechanisms responsible for this remain unclear. Here, we identified cell-type-specific transcriptional signatures associated with a sustained ketamine response in mice. Most interestingly, we identified the *Kcnq2* gene as an important downstream regulator of ketamine action in glutamatergic neurons of the ventral hippocampus. We validated these findings through a series of complementary molecular, electrophysiological, cellular, pharmacological, behavioral, and functional experiments. We demonstrated that adjunctive treatment with retigabine, a KCNQ activator, augments ketamine's antidepressant-like effects in mice. Intriguingly, these effects are ketamine specific, as they do not modulate a response to classical antidepressants, such as escitalopram. These findings significantly advance our understanding of the mechanisms underlying the sustained antidepressant effects of ketamine, with important clinical implications.

## INTRODUCTION

The discovery that a single sub-anesthetic dose of ketamine, a glutamate N-methyl-D-aspartate (NMDA) receptor blocker, produces a rapid yet sustained antidepressant response, even in treatment-resistant patients, is one of the most significant improvements in the field of depression in over 60 years (Duman, 2018; Yang et al., 2018). Ketamine is effective for the treatment of suicidal ideation in emergency room settings, and its antidepressant effects have been demonstrated in many human and animal studies (Krystal et al., 2019). Despite these encouraging clinical and preclinical findings, controversy remains regarding ketamine's efficacy in treating major depressive disorder (MDD) (Gastaldon et al., 2019). This has encouraged research into ketamine's mechanisms of action in an effort to understand its primary and downstream targets, so that better treatment interventions for depression can be developed.

Previous studies have investigated the molecular mechanisms underlying the antidepressant effects of ketamine, and several mechanisms of action have been proposed (Aleksandrova et al., 2017). However, given that the antidepressant effects of ketamine remain long after its metabolism, its mechanism of action cannot be solely attributed to ketamine's ability to inhibit NMDR or increase the function of $\alpha$-amino-3-hydroxy-5-methyl-4-isoxazolepropionic acid receptors (AMPAR). Instead, it may result from the activation of downstream signaling cascades causing long-lasting and sustained adaptations in key brain areas and neural circuits. Despite the progress (Zanos and Gould, 2018), the exact mechanism of ketamine action is still not fully understood. It is possible that some of the more elusive molecular components of this mechanism remain unclear due to important methodological limitations, specifically the absence of cell-type-specific information (Gururajan et al., 2018). Previous gene expression (GE) studies provided data

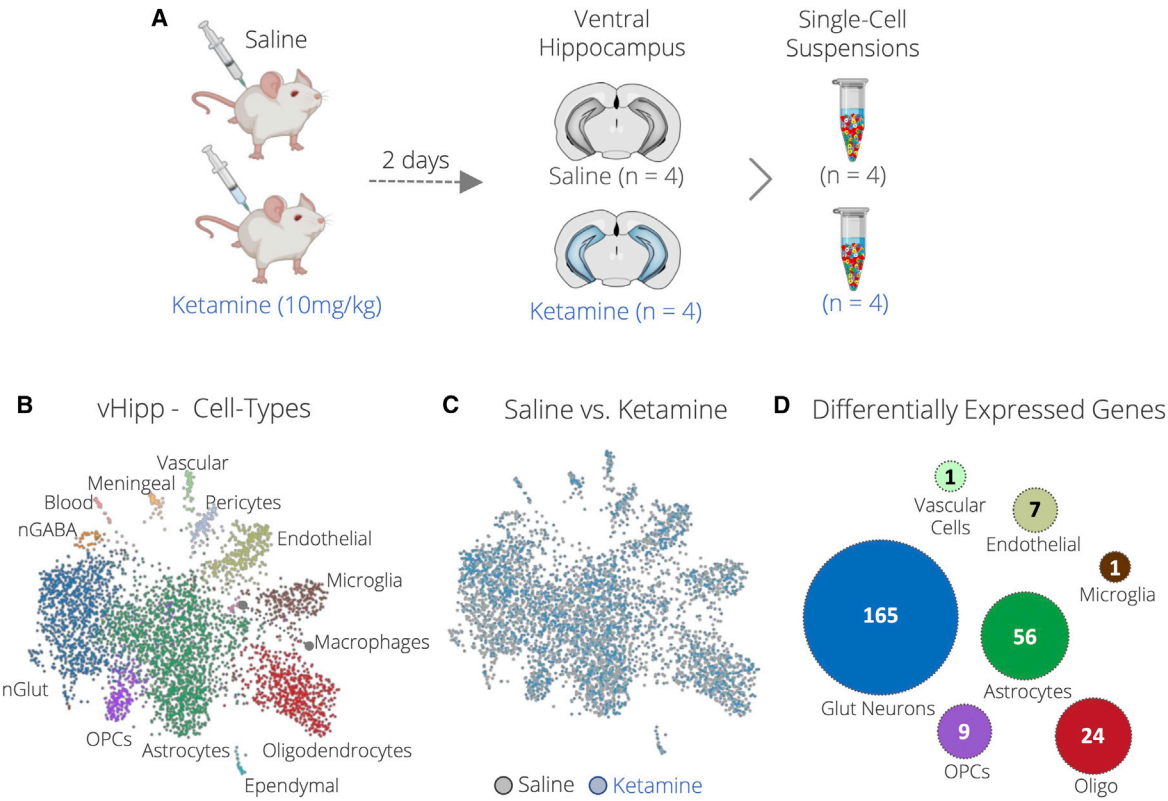


**Figure 1. Cell-type-specific transcriptomic characterization of the ventral hippocampus after ketamine treatment**

(A) Mice were injected with ketamine (10 mg/kg/BW) or saline and sacrificed 2 days post-injection. Cell suspensions were prepared from the ventral hippocampus (vHipp) of ketamine (n = 4) and saline-treated controls (n = 4).

(B) UMAP plot depicting single cells from the vHipp. Colors represent each of the 13 clusters of individual cell types identified as glutamatergic neurons (nGlut), GABAergic neurons (nGABA), oligodendrocytes, oligodendrocyte progenitor cells (OPCs), astrocytes, endothelial, microglia, macrophages, ependymal, pericytes, meningeal, vascular cells, and blood cells.

(C) Distribution of single cells by treatment: saline (gray) and ketamine (blue).

(D) Differentially expressed genes in 7 clusters of the vHipp. See also Figure S1; Tables S1–S3.

from brain homogenates; thus, any treatment response signature specific to a particular cell type is averaged out (Bagot et al., 2017; Duman et al., 2019; Ficek et al., 2016; Ho et al., 2019; Kim et al., 2021; Mastrodonato et al., 2018; Nasca et al., 2015).

In this study, using single-cell RNA sequencing (scRNA-seq), we comprehensively cataloged the transcriptome of thousands of ventral hippocampus (vHipp) cells of mice treated with a single dose of (*R*,*S*)-ketamine or a saline vehicle control and found cell-type-specific transcriptional signatures associated with the sustained antidepressant effects of ketamine. Notably, we identified *Kcnq2* as an important downstream regulator of ketamine action in glutamatergic neurons of the vHipp. These findings were validated using glutamatergic neurons sorted from a conditional reporter mouse line, *in vitro* treatment of primary hippocampal neurons, electrophysiological recordings *in vitro* and from acute vHipp slices, a validated mouse chronic stress model for depression, as well as a viral-mediated knockdown of *Kcnq2* in the vHipp of mice. In addition, we identified a previously unknown mechanism of action for ketamine via *Kcnq2* in glutamatergic neurons of the hippocampus.

We demonstrated that (1) systemic pharmacological manipulation of KCNQ channels modulates antidepressant behaviors in mice, (2) adjunctive treatment with retigabine, a KCNQ activator, augments ketamine's effects, and (3) the effects of KCNQ are specific to ketamine, as they do not modulate the response to classical antidepressants. We provided new insights into the molecular mechanisms underlying the sustained antidepressant effects of ketamine and postulated the voltage-gated potassium channel KCNQ as a downstream regulator of ketamine action, as well as a promising target for the development of MDD treatments.

## RESULTS

### scRNA-seq reveals cell-type-specific molecular signatures of ketamine treatment in the vHipp

To characterize cell-type-specific molecular changes associated with the sustained antidepressant effects of ketamine, we treated mice with either ketamine or a saline control. Brains were collected 2 days post-treatment, and single-cell suspensions were prepared for scRNA-seq (Figure 1A). The transcriptome of thousands of single cells from the vHipp, a well-known

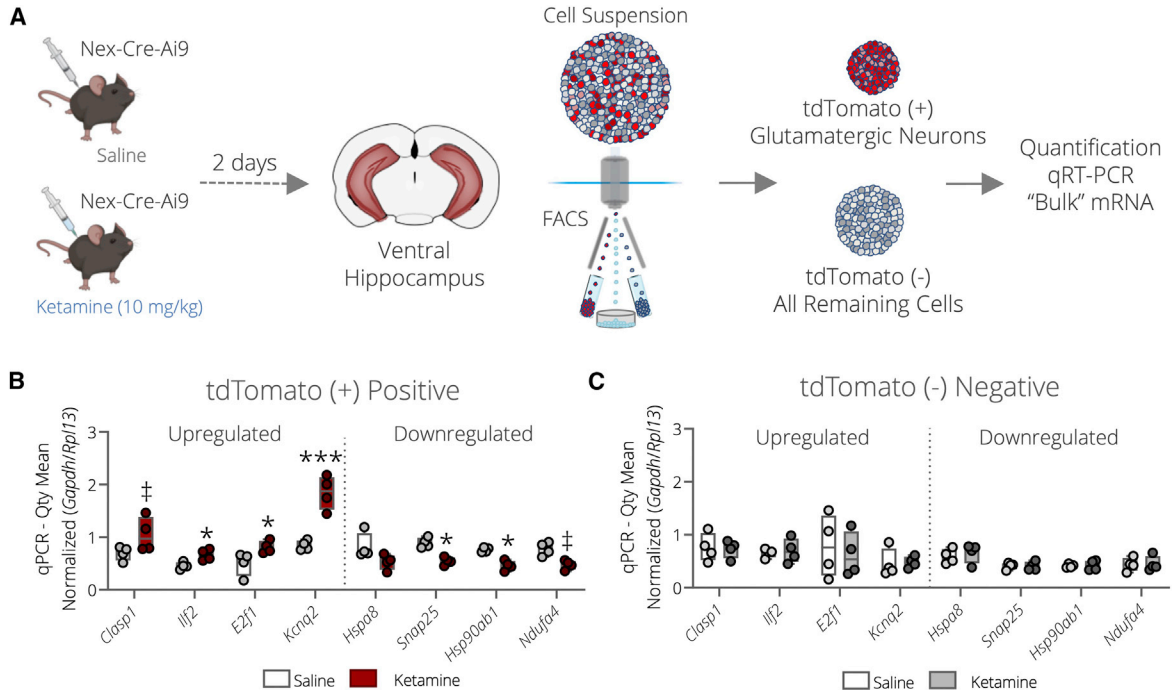


**Figure 2. Validation of single-cell RNA-seq data via FACS**

(A) Nex-Cre-Ai9 mutant mice were injected with ketamine (10 mg/kg/BW) (n = 4) or a saline solution (n = 4). After 2 days, individual cell suspensions were prepared from the vHipp of all mice. Glutamatergic neurons (tdTomato+) and all remaining cell types (tdTomato) from the vHipp were isolated using FACS.

(B and C) Boxplots represent qPCR mRNA levels of 8 (4 upregulated and 4 downregulated) DEGs in tdTomato+ (red) and tdTomato− (gray) cells between ketamine- and saline-treated mice. (n = 4, per condition). All qPCR data were normalized to the combined mRNA expression of the endogenous controls, *Gapdh* and *Rpl13*. Data represented as mean ± SEM. One-way ANOVA. Multiple testing was corrected using the Benjamini-Hochberg method. ***$p < 0.001$, *$p < 0.05$, ‡$p < 0.1$. See also Figure S2.

region for ketamine antidepressant action in rodents and humans, was sequenced (Ionescu et al., 2018; Kraguljac et al., 2017; Zanos and Gould, 2018). After quality control and preprocessing (Figure S1A), single cells were grouped according to their GE profiles using graph-based clustering. Uniform manifold approximation and projection (UMAP) plots were used to visualize clusters. Our unsupervised cluster analysis revealed 13 cell clusters with distinct GE signatures (Figures 1B and S1B). We found no significant differences in the relative cell-type composition for each cluster between the ketamine- and saline-treated groups (Figure 1C; Table S1). Subsequently, we performed differential expression analyses to evaluate cell-type-specific molecular signatures of ketamine action (see STAR Methods). We identified a total of 263 differentially expressed genes (DEGs) in 7 of the 13 clusters, ranging from 1 to 165 DEGs per cell type (Figure 1D; Table S2). We found that 31 of the 263 DEGs were significantly dysregulated in more than 1 cluster; however, 135 DEGs were exclusively in glutamatergic (GLUT) neurons, 27 in astrocytes, 16 in oligodendrocytes, 3 in oligodendrocyte progenitor cells (OPCs), 1 in endothelial cells, and 1 in vascular cells (Figure S1C; Table S3). Additionally, we performed a pathway enrichment analysis for the three cell types with the largest DEGs, using Enrichr (Xie et al., 2021). In GLUT neurons, our analysis revealed many significant pathways involved in calcium signaling, synaptic function and plasticity, and neurodevelopmental disorders (Figure S1D). Astrocytes showed an enrichment for fatty acid elongation, gap junction, phagosome activity, and Alzheimer's disease (Figure S1E), whereas oligodendrocytes showed an enrichment for vitamin digestion, absorption, and fatty acid elongation (Figure S1F).

The GLUT neurons were the most interesting cell type based on their multigenic response (165 DEGs) (Figure 1D) and their known role in modulating the antidepressant effects of ketamine (Duman et al., 2019; Lur et al., 2019; Pothula et al., 2021). Next, we generated a conditional reporter mouse line (*Nex-Cre-Ai9*) where most GLUT neurons of the forebrain, including the hippocampus, are fluorescently labeled by tdTomato (Figure S2A) (Hartmann et al., 2017). Mice were injected with ketamine or a saline control. The vHipp was dissected 2 days post-injection (Figure 2A). Individual whole cells were sorted using fluorescence-activated cell sorting (FACS) into two separate pools of cells from each mouse. One pool contained GLUT neurons (tdTomato+), and the other contained all other vHipp cell types (tdTomato−) (Figures 2A and S2B–S2D). To confirm the presence of GLUT neurons in the tdTomato+ pool, we quantified mRNA and found higher levels of the genes coding for *Neurod6*, tdTomato, as well as *Slc17a7*, a known marker of GLUT neurons, as compared with the tdTomato− pool (Figure S2E). We quantified mRNA of the established cell-type-specific markers *Slc32a1* (GABAergic neurons), *Slc1a3* (astrocytes), *Mog* (oligodendrocytes), *C1qc* (microglia), and *Cldn5* (endothelial cells) and found that tdTomato+ cells expressed lower levels of these genes, as

compared with tdTomato− cells (Figure S2E), confirming the presence of GLUT neurons in the tdTomato+ cells. We used these two pools to validate our scRNA-seq findings at the population level, using quantitative real-time polymerase chain reaction (qPCR). We found no significant differences in the total number of tdTomato+ cells from the ketamine or saline groups, confirming our scRNA-seq results (Figures S2F–S2H). As a proof of principle, we selected 8 of the top DEGs in GLUT neurons (4 upregulated and 4 downregulated) from our scRNA-seq analysis (Table S2). We found that most of the genes quantified in the tdTomato+ cells were significantly dysregulated and directionally consistent with our scRNA-seq findings (Figure 2B). The voltage-gated potassium channel subfamily Q member 2 (*Kcnq2*) showed the strongest effect after ketamine treatment ($p < 0.001$, FC = 2.2). We found no significant differences in mRNA levels for any of the 8 DEGs in the tdTomato− cells (Figure 2C).

To compare whole tissue "bulk" versus cell-type-specific methods, we quantified the mRNA expression of these 8 genes using brain punches from the vHipp of a new cohort of mice. Our results showed small changes in a direction that was consistent with our scRNA-seq results; however, these effects did not reach statistical significance (Figures S2I and S2J). Overall, these results show that ketamine elicits sustained cell-type-specific GE changes in the vHipp of mice and that these changes are masked in bulk analyses.

## Ketamine treatment regulates *Kcnq2* in primary hippocampal neurons

Next, we examined whether a single ketamine treatment of primary hippocampal neurons could modify the mRNA expression of the 8 genes tested earlier. Mouse primary hippocampal neurons are mostly made up of GLUT neurons and therefore make a very good model system to further validate our previous *in vivo* findings. Primary neurons were cultured for 21 days and then stimulated with a single dose of ketamine (10 μM) or its active metabolite, (2*R*, 6*R*)-hydroxynorketamine (HNK) (10 μM). These concentrations were selected after careful experimental consideration and review of the available literature (Figures S3A–S3G). Following the treatment, neurons were collected 2, 12, 24, or 48 h later and compared with untreated and saline controls (Figure 3A). We found no significant differences in the expression of any of the 8 genes tested after treatment with a saline control, as compared with the untreated primary neurons (Figure 3A). However, we found significant changes in the mRNA expression of 7 out of 8 genes after ketamine treatment, which were directionally consistent with our scRNA-seq findings (Figure 3A). Among the DEGs, *Kcnq2* displayed the largest changes in GE after treatment, showing a significant upregulation at all time points. Our findings suggest that *Kcnq2* is transcriptionally regulated by ketamine and could be an important downstream regulator of ketamine action in glutamatergic neurons of the vHipp.

## Ketamine increases KCNQ channel currents in hippocampal neurons *in vitro* and *in vivo*

The *Kcnq2* gene encodes for the Kv7.2 protein, a slow-acting, voltage-gated potassium channel that plays a critical role in the regulation of neuronal excitability (Jentsch, 2000). The Kv7.2 and Kv7.3 proteins (*Kcnq3* gene) can form KCNQ (Kv7) homo- or heterotetramers that generate a signature M-current, modulating the overall excitability of neurons (Barrese et al., 2018; Cooper and Jan, 2003). To investigate the KCNQ channel as a mediator of the sustained antidepressant effects of ketamine, we treated mouse primary hippocampal neurons with HNK (10 μM) or a saline control for 24 h and quantified M-current density ($I_M$) using whole-cell voltage-clamp recordings (Figure 3B). Neurons treated with HNK displayed a significant increase in $I_M$ current density versus saline-treated controls (Figures 3C and 3D). Next, we performed *ex vivo* patch-clamp recordings from acute hippocampal slices to test the effects of ketamine treatment on $I_M$ current density (Figure 3E). Briefly, mice were injected with ketamine or a saline control and sacrificed 2 days later. Electrophysiological recordings were taken specifically from glutamatergic (CA1 pyramidal) neurons of the vHipp. Similarly to our *in vitro* findings, ketamine-treated mice showed a significant increase in $I_M$ current density versus saline-treated controls (Figures 3F, 3G, S3H, and S3I), suggesting that ketamine increases the expression of KCNQ channels *in vivo*. These findings indicate that the increased *Kcnq2* mRNA expression observed in glutamatergic neurons 2 days after ketamine treatment is accompanied by a significant gain in the number of functional KCNQ channels expressed in GLUT neurons of the hippocampus both *in vitro* and *in vivo*. Together, our findings further support the idea that KCNQ channels are a downstream regulator of sustained ketamine action and suggest that modulation of these channels in GLUT neurons of the vHipp could be a potential target for MDD treatment.

## shRNA knockdown of *Kcnq2* in the vHipp reduces the antidepressant effects of ketamine

The M channel (KCNQ) is formed by the proteins encoded by the *Kcnq2* and *Kcnq3* genes, both integral membrane proteins (Baculis et al., 2020). We did not find any significant differences in the mRNA expression of *Kcnq3* after ketamine treatment in our original cohort, our FACS-sorted sample, or in primary hippocampal neurons (Figures S4A–S4C; Table S2), suggesting that ketamine produces an effect specific to *Kcnq2*, but not to *Kcnq3*. To explore the expression of *Kcnq2* and *Kcnq3* in the brain, we examined publicly available *in situ* hybridization (ISH) data from 12 different regions of the mouse brain (Lein et al., 2007). *Kcnq2* shows its highest expression in the hippocampus formation, whereas *Kcnq3* is highly expressed throughout multiple brain regions (Figures S4D–S4F). In addition, our single-cell data, as well as other publicly available single-cell datasets, show that *Kcnq2* is exclusively expressed in neurons, whereas *Kncq3* is expressed in neurons, astrocytes, oligodendrocytes, and OPCs (Lopez et al., 2021; Tasic et al., 2018; Zeisel et al., 2018) (Figures S5A–S5F). These findings reinforce the idea that *Kcnq2* plays an important and more centralized role in neurons of the hippocampus, making this region a good candidate for *in vivo* viral manipulations. To functionally explore the role of *Kcnq2* in mediating the antidepressant effects of ketamine, we designed adeno-associated virus (AAV) constructs to knock down *Kcnq2 in vivo* (Figure 4A). Transfection of Neuro2a (N2a) cultured cells and viral injection into the vHipp of adult mice resulted in a significant decrease in *Kcnq2* mRNA levels, both

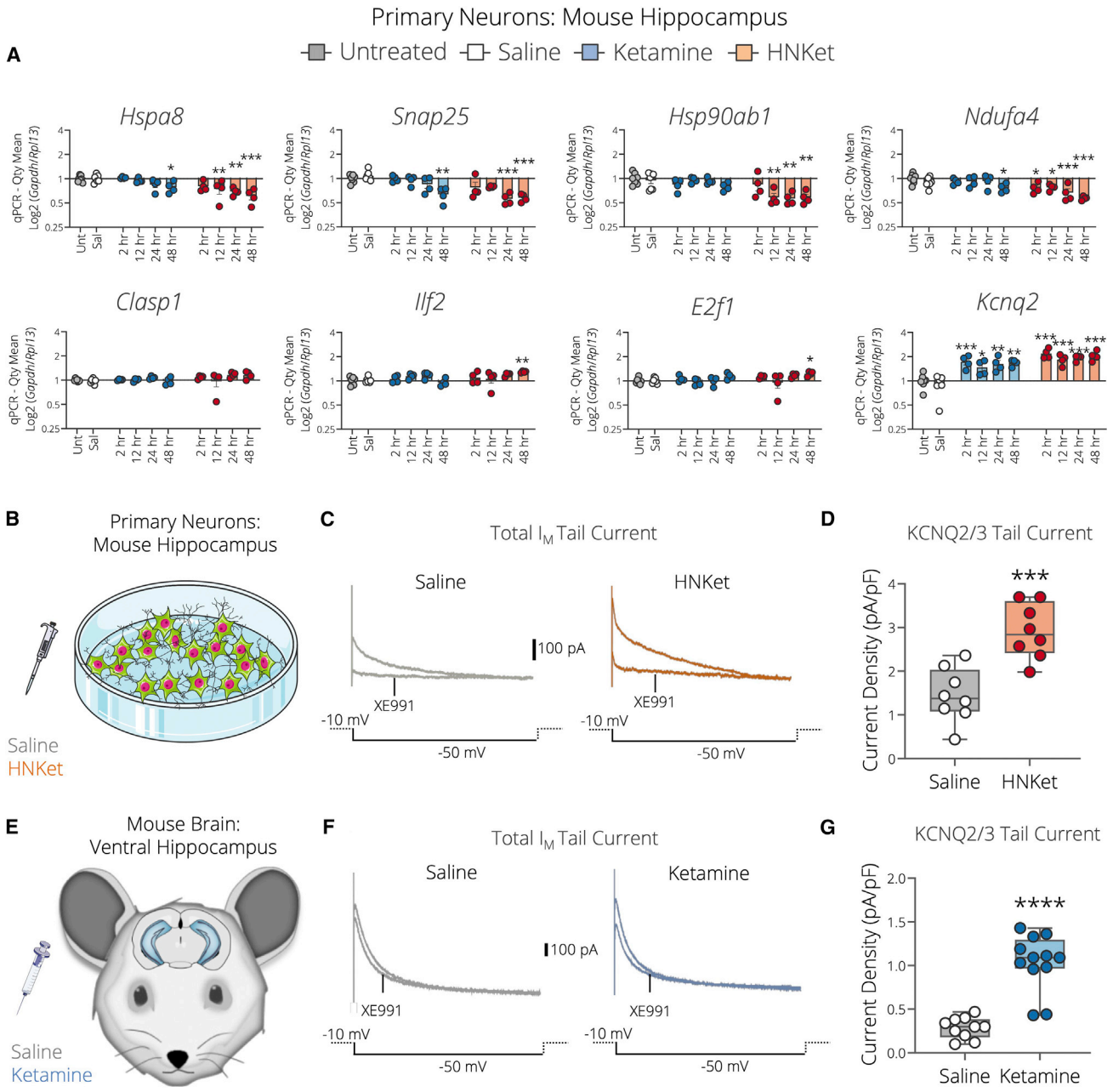


**Figure 3. Effects of ketamine and HNK stimulation *in vitro* and *ex vivo***

(A) Primary hippocampal neurons treated with a single dose of either ketamine (10 μM), HNK (10 μM), or a saline control. Neurons were collected after 2, 12, 24, or 48 h post-injection (n = 4, per condition). Bar plots represent qPCR mRNA levels. All qPCR data were $\log_2$-transformed and normalized to the geometric mean of *Gapdh* and *Rpl13*. One-way ANOVA. Multiple testing was corrected using the Benjamini-Hochberg method.

(B–G) Electrophysiological analysis of $I_M$ tail current density in primary hippocampal neurons and CA1 pyramidal cells from the vHipp in acute brain slices. (B) Primary cultures were treated with saline (gray) or HNK (10 μM, orange red) and assessed 24 h after treatment. (E) vHipp slices were obtained from CD1 mice that received an injection of saline (gray) or ketamine (10 mg/kg/BW) (blue), 2 days before slice preparation. Total $I_M$ tail current (C and F): representative current traces from whole-cell voltage-clamp recordings describe the amplitude of the total $I_M$ tail current as obtained during recordings. KCNQ2/3 tail current (D and G): boxplots represent the isolated KCNQ2/3 current density (pA/pF), which is the current amplitude of the $I_M$ current carried specifically by KCNQ2/3 and divided by the cell capacitance. *In vitro* (n = 8 cells for each group from 2 independent cultures, gray = saline; orange = HNK). *Ex vivo* (gray: n = 5, 10 cells; blue: n = 6, 12 cells). n = number of mice (biological replicates). Data represented as mean ± SEM. Unpaired t tests, two tailed. ***p < 0.001, **p < 0.01, *p < 0.05. See also Figure S3.

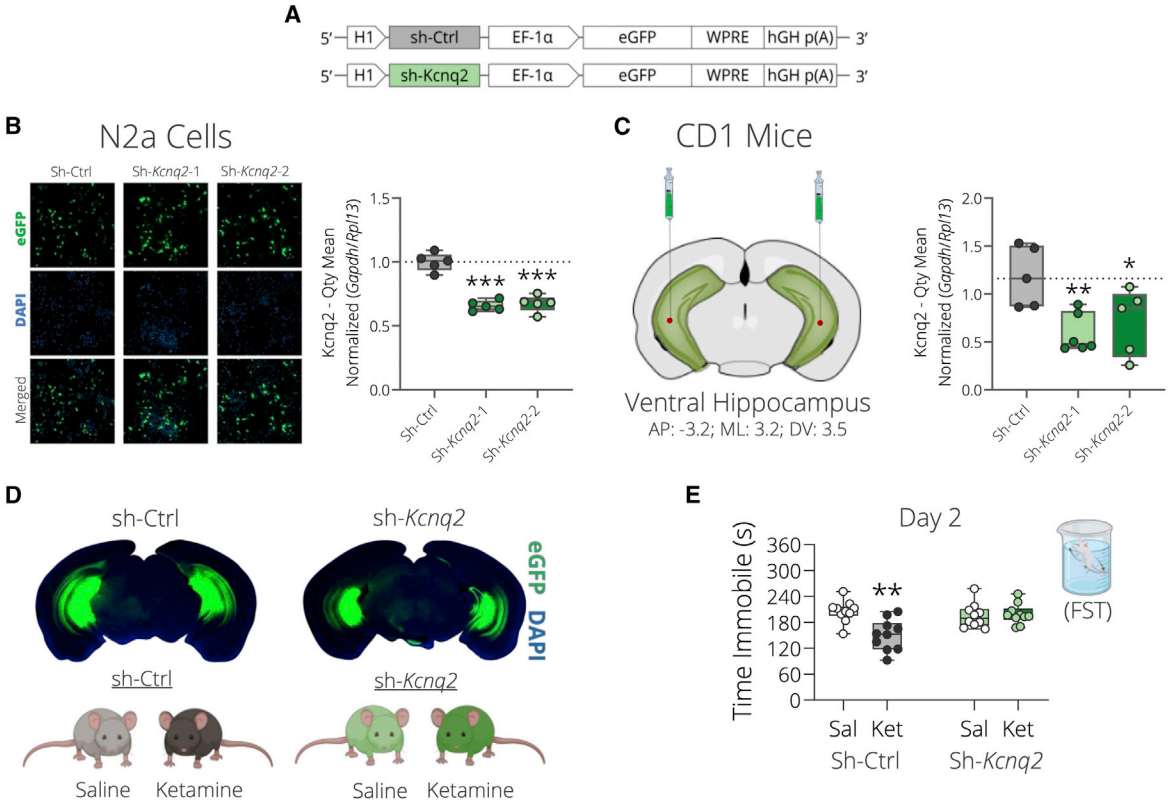


**Figure 4. *In vivo* manipulation of *Kcnq2* in the mouse ventral hippocampus modulates antidepressant-like behaviors**

(A) Schematic overview of the *Kcnq2* knockdown (green) and control (gray) construct with eGFP and shRNA driven by EF1a and H1 promoter.

(B) Representative images of N2a cells transfected with an shRNA control or two different shRNA-*Kcnq2* vectors (n = 5, per condition). Fluorescent eGFP signal (green); DAPI signal (blue). Boxplots represent qPCR mRNA expression levels of *Kcnq2*. One-way ANOVA, corrected for multiple comparisons.

(C) Coronal map with the region and bregma coordinates (mm) targeted for *in vivo* viral manipulation. AP anteroposterior, ML mediolateral, DV dorsoventral. Bar plots represent qPCR mRNA expression levels (n = 5, per condition). qPCR data were normalized to the geometric mean of *Gapdh* and *Rpl13*. One-way ANOVA. Multiple testing was corrected using the Benjamini-Hochberg method.

(D) Representative images of mouse brains injected with shRNA-*Kcnq2* and shRNA control AAV. Fluorescent eGFP signal (green); DAPI signal (blue). Mice were injected in the vHipp (bilateral) with either shRNA-*Kcnq2* (n = 22) or shRNA control (n = 19) AAV. 4 weeks after viral injection, mice were randomly selected to receive a ketamine (10 mg/kg/BW) or saline injection.

(E) Boxplots represent total immobile time (S) during the forced swim test (FST) in mice that received shRNA-Ctrl (gray) or shRNA-*Kcnq2* (green) after ketamine (dark green) or saline injection (dark gray) (n = 10, per condition). The FST was performed 2 days after treatment. Data represented as mean ± SEM. Two-way ANOVA. Multiple testing was corrected using the Benjamini-Hochberg method ***$p < 0.001$, **$p < 0.01$, *$p < 0.05$. See also Figures S4–S6.

*in vitro* and *in vivo* (Figures 4B and 4C). We injected shRNA-*Kcnq2* or shRNA-scramble control AAVs bilaterally into the vHipp of a new cohort. Four weeks after viral injection, half of the mice were randomly selected to receive a ketamine or saline injection, and the antidepressant effects of ketamine were assessed using the forced swim test (FST), a validated test for evaluating antidepressant efficacy in rodents (Yankelevitch-Yahav et al., 2015) (Figures 4D and 4E). In the group of mice treated with an shRNA-scramble control, we found a significant decrease in immobility time during the FST in mice treated with ketamine versus controls (Figure 4E, left). Notably, the antidepressant effects of ketamine were no longer detected in mice expressing the shRNA-*Kcnq2* virus (Figure 4E, right). We also assessed locomotor activity to rule out any confounding effects of hyperlocomotion in the FST after ketamine treatment and found no differences in total activity between groups (Figures S6A and S6B). These results indicate that the vHipp is an important site for *Kcnq2* function and the sustained antidepressant effects of ketamine.

## Chronic stress exposure and ketamine treatment modulate *Kcnq2* mRNA in the vHipp

To further investigate the role of *Kcnq2* in GLUT neurons of the vHipp, a new group of *Nex-Cre-Ai9* mice was subjected to the chronic social defeat stress (CSDS) model, a validated paradigm to induce long-lasting depression- and anxiety-like endophenotypes in mice (Figure 5A) (Lopez et al., 2021). 10 days of CSDS exposure led to hallmark features of chronically stressed mice (Figures S6C–S6F). In the FST, chronically stressed mice showed a significant increase in immobility time, as compared with non-stressed controls (Figure 5B). Endpoint and tissue collection were performed 24 h after the last social defeat session (day 11), thus capturing the cumulative effects of chronic stress, rather than any acute effects of the last defeat. The vHipp

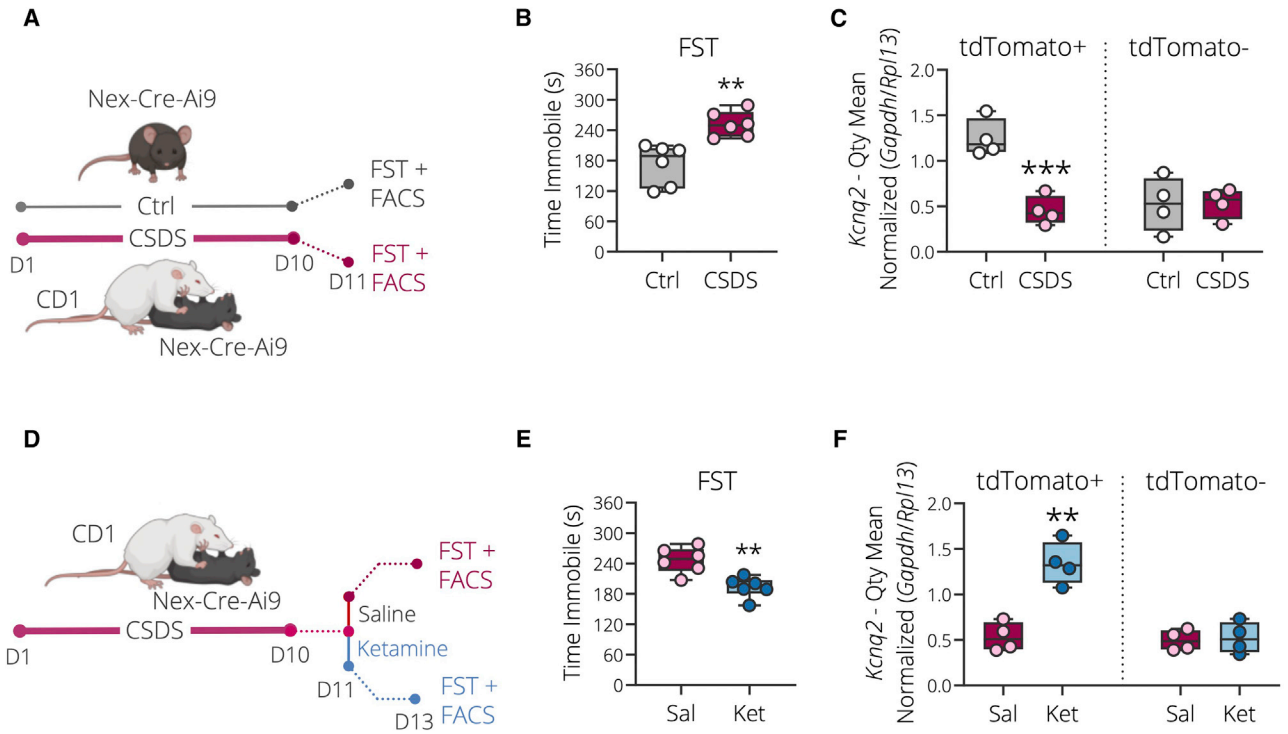


**Figure 5. Chronic stress exposure and ketamine modulate *Kcnq2* mRNA in the ventral hippocampus**

(A) Experimental timeline of CSDS for control and stressed mice.

(B) Boxplots represent total immobile time (s) during the FST in non-stressed controls (n = 6, gray) and CSDS mice (n = 6, purple). Unpaired t test, two tailed.

(C) Boxplots represent qPCR mRNA levels of *Kcnq2* in tdTomato+ and tdTomato− cells between non-stressed controls (n = 4, gray) and CSDS mice (n = 4, purple). One-way ANOVA. Multiple testing correction was performed using the Benjamini-Hochberg method.

(D) Experimental timeline of CSDS paradigm plus treatment.

(E) Boxplots represent total immobile time (s) during the FST in chronically stressed mice who received a saline (n = 6, purple) or ketamine (n = 6, blue) treatment. Unpaired t test, two tailed.

(F) Boxplots represent qPCR mRNA levels of *Kcnq2* in tdTomato+ and tdTomato− cells between chronically stressed mice that received a saline (n = 4, purple) or ketamine (n = 4, blue) treatment. One-way ANOVA. Multiple testing was corrected using the Benjamini-Hochberg method. Data represented as mean ± SEM. ***p < 0.001, **p < 0.01. See also Figure S6.

was dissected, and individual cells were sorted (as described in Figure 2A). We found that *Kcnq2* mRNA expression was decreased only in GLUT neurons (tdTomato+) of the vHipp, as we did not find any significant differences in the remaining cell types (tdTomato−) (Figure 5C). We also found a significant difference in *Kcnq2* mRNA expression between tdTomato+ and tdTomato− cells, confirming that *Kcnq2* is enriched in GLUT neurons of the vHipp. Finally, to access bulk mRNA expression levels of *Kcnq2* following chronic stress, we quantified its expression in vHipp brain punches from a new cohort of chronically stressed and control mice. Although there was a decrease in *Kcnq2* mRNA levels in stressed mice versus controls, it did not reach statistical significance (Figure S6G; p = 0.08).

In order to test whether CSDS-induced *Kcnq2* decrease can be reversed by ketamine treatment, we exposed a new group of *Nex-Cre-Ai9* mice to the CSDS model. On day 11, mice were treated with either ketamine or a saline control (Figure 5D). The antidepressant effects of ketamine were assessed 2 days after treatment (day 13), using the FST. In addition, the vHipp of saline- and ketamine-treated CSDS mice were dissected, and individual cells were sorted using FACS. Interestingly, ketamine reversed the effects of chronic stress in the FST (Figure 5E) and *Kcnq2* mRNA in GLUT neurons (Figure 5F). *Kcnq2* mRNA expression was significantly increased to baseline levels (as seen in non-stressed controls, Figure 5C) in ketamine-treated CSDS mice versus saline-treated controls (Figure 5F). In addition, these effects were specific to GLUT neurons (tdTomato+) of the vHipp (Figure 5F, left), since we did not find any significant differences in tdTomato− cells (Figure 5F, right). We found no significant increase in *Kcnq2* mRNA in ketamine-treated CSDS mice using bulk mRNA (Figure S6H). These results demonstrate that *Kcnq2* mRNA is altered after chronic stress exposure in GLUT neurons of the vHipp and that these effects can be reversed by ketamine treatment. Furthermore, these cell-type-specific effects could be diluted or distorted when using brain homogenates.

## Ketamine regulates *Kcnq2* mRNA via $Ca^{2+}$ and calmodulin/calcineurin signaling

Having identified *Kcnq2* as a downstream regulator of the sustained antidepressant effects of ketamine, we wanted to further investigate how ketamine transcriptionally upregulates *Kcnq2*

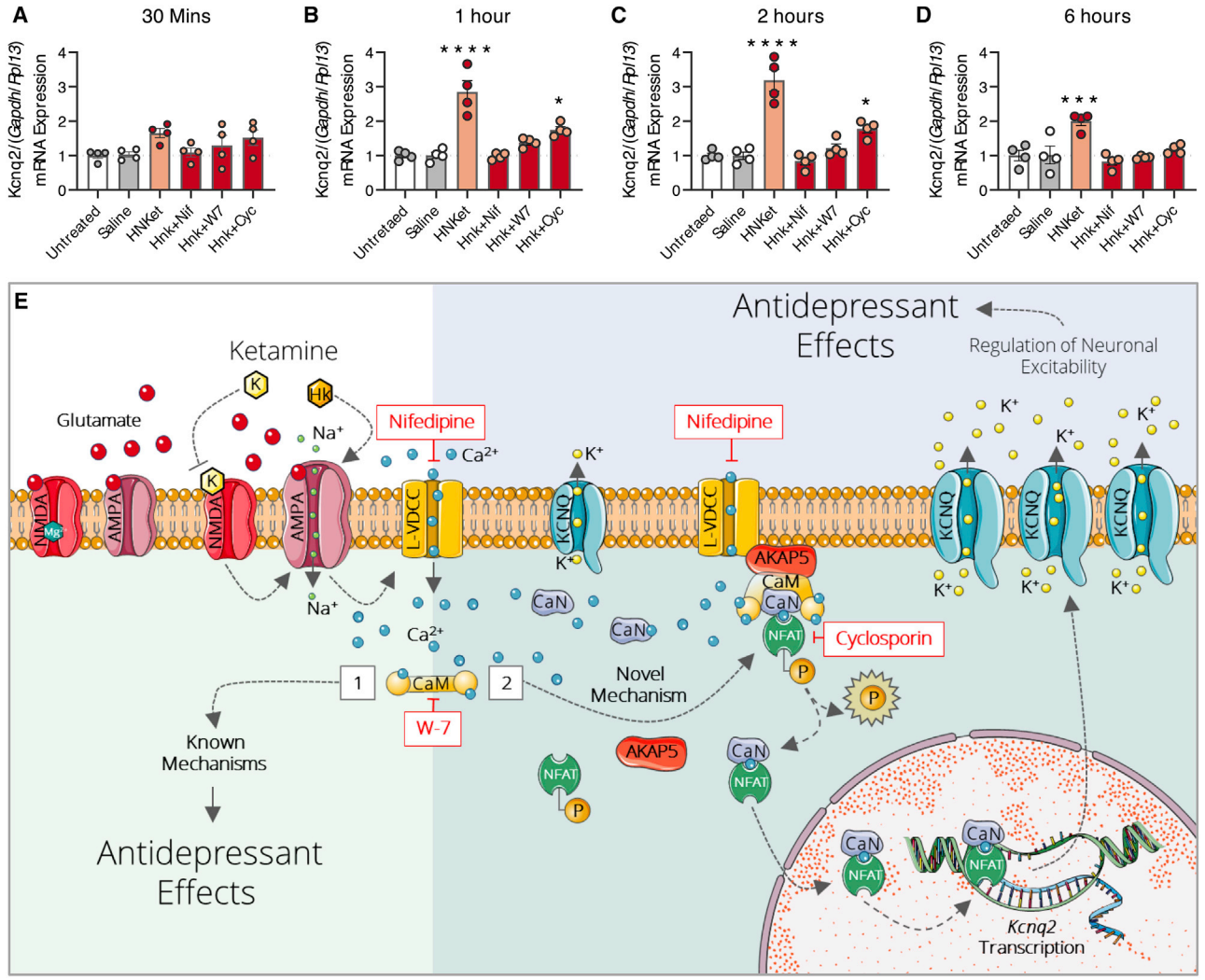


**Figure 6. Ketamine regulates *Kcnq2* via calcium/calmodulin and AKAP5 signaling**

(A–D) Hippocampal primary neurons (mouse) stimulated with either saline solution, HNK (10 μM), or a combination of HNK and nifedipine (calcium channel blocker), W-7 hydrochloride (calmodulin inhibitor), or cyclosporine-A (calcineurin inhibitor) for 30 min, 1, 2, or 6 h, and compared with an untreated control. n = 4 (biological replicates) per condition and treatment. Boxplots represent qPCR mRNA levels of *Kcnq2*. One-way ANOVA. Multiple testing was corrected using the Benjamini-Hochberg method. Data represented as mean ± SEM. ****$p < 0.0001$, ***$p < 0.001$, *$p < 0.05$.

(E) Schematic model for transcriptional regulation of *Kcnq2*. NMDAR inhibition (via ketamine) or increased AMPAR function (via HNK) leads to an increase in L-type calcium channel (L-VDCC) activity, creating elevated levels of intracellular calcium ($Ca^{2+}$) leading to (1) the already known mechanisms of ketamine action or (2) a novel mechanism via transcriptional regulation of *Kcnq2* mRNA by the Akap5-CaM-CaN complex.

mRNA to exert its sustained antidepressant-like effects. Previous studies have successfully shown that *Kcnq2* mRNA can be regulated via calmodulin (CaM), calcineurin (CaN), and the A-kinase-anchoring protein 5 (AKAP5) (Zhang and Shapiro, 2012; Zhou et al., 2016). This complex activates the transcription factor NFAT (nuclear factor of activated T cells), which acts on *Kcnq2* gene regulatory elements, as opposed to *Kcnq3* (Zhang and Shapiro, 2012). As a result, enhanced and sustained *Kcnq2* transcription leads to increased M channel activity and regulation of neuronal excitability. Interestingly, the CaM genes, *Calm1* and *Calm2*, as well as *Akap5*, were among the DEGs of our scRNA-seq analysis (Table S2). Having already shown that ketamine increases the mRNA expression of *Kcnq2* in primary hippocampal neurons (Figure 3A), we next wanted to investigate whether ketamine regulates *Kcnq2* mRNA via $Ca^{2+}$, CaM, CaN, or AKAP5 signaling. We used pharmacological inhibition of the key components of this pathway to see whether it interferes with the upregulation of *Kcnq2* mRNA by a single ketamine treatment *in vitro*. Primary hippocampal neurons were stimulated with a single dose of either saline, HNK, or a combination of HNK plus nifedipine (L-type $Ca^{2+}$ channel blocker), W-7 hydrochloride (CaM inhibitor), or cyclosporine-A (CaN inhibitor). Neurons were collected at 4 time points: 30 min, 1, 2, or 6 h (post-treatment) and compared with a group of untreated controls (Figures 6A–6D). We did not find any significant differences in the expression of *Kcnq2* mRNA 30 min after treatment

(Figure 6A). However, consistent with our results (Figure 3A), we found a significant upregulation of *Kcnq2* mRNA 1, 2, and 6 h after a single treatment with HNK (Figures 6B–6D). Interestingly, blockade of L-type $Ca^{2+}$ channels and CaM by nifedipine and W-7, respectively, eliminated the upregulation of *Kcnq2* by ketamine at all time points tested (Figures 6B–6D). In contrast, inhibition of CaN only abolished the effects of ketamine on *Kcnq2* mRNA 6 h after treatment (Figure 6D). These results, summarized in Figure 6E, suggest that *Kcnq2* mRNA changes are not directly or immediately induced after ketamine treatment but the result of downstream events initiated by ketamine. Furthermore, our findings show that the ketamine-induced increase in the expression of *Kcnq2* mRNA was blocked by nifedipine, W-7, or cyclosporine-A, suggesting a critical role for L-type $Ca^{2+}$ channels, CaM, and CaN in the transcriptional regulation of *Kcnq2* by ketamine treatment at later time points.

### Pharmacological manipulation of KCNQ modulates antidepressant-like behaviors in mice

Previous studies in rodents have shown that KCNQ function can be regulated with highly specific agonists and antagonists (Barrese et al., 2018). To further explore the KCNQ channel as a potential therapeutic target of ketamine, we examined whether pharmacological inhibition of KCNQ alone or in combination with ketamine had any effects on behavior. Mice received two injections with a combination of drugs. We first treated mice with XE991, a potent and selective KCNQ (*Kcnq2/3*) channel inhibitor (Greene et al., 2017), using different concentrations (1 and 3 mg/kg/BW), in the absence or in combination with ketamine and compared them with saline-treated controls. To assess the behavioral effects elicited by ketamine, XE991, and its combination, we exposed these mice to a FST (Figure 7A, left). As expected, we found a significant decrease in immobility time during the FST in mice treated with ketamine, as compared with saline-treated mice (Figure 7B). We did not find any significant differences in mice that received XE991 in combination with saline (Figure S6I), suggesting that XE991 alone does not produce any acute behavioral effects in the FST. Consistent with our hypothesis, the antidepressant effects of ketamine were abolished in mice that were treated with both XE991 and ketamine (Figures 7B and S6I). These results indicate that KCNQ activity might be necessary for ketamine to exert its antidepressant actions. We then sought to test whether we could mimic, increase, or amplify the effects of ketamine using retigabine, a selective KCNQ (*Kcnq2/3*) channel activator (Kalappa et al., 2015). As in the previous experiment, mice were treated with saline, ketamine, or ketamine in combination with two different concentrations of retigabine (1 and 5 mg/kg) (Figure 7A, right). Again, we observed a significant effect of ketamine as compared with saline controls in the FST (Figure 7C). We did not find any effects of retigabine when it was administered in combination with saline alone (Figure S6J). However, in combination with ketamine, retigabine (1 mg/kg) produced a stronger effect in the FST that was significantly different versus ketamine alone (FC: 0.71, $p = 0.0001$) (Figures 7C and S6J). Interestingly, the combined administration of ketamine and retigabine at a higher dose (5 mg/kg) did not produce any acute behavioral effects in the FST. This is in line with ketamine's inverted U-shaped dose response (Li et al., 2010). These results suggest that pharmacological manipulation of KCNQ modulates antidepressant-like behavior.

### Ketamine and retigabine modulate antidepressant-like behaviors in a seminaturalistic living environment

Next, we used the "social box" (SB) to assess the sustained antidepressant effects of ketamine. The SB system is ideally suited for in-depth investigations of pharmacological manipulations, since it allows long-term, continuous tracking of the social behaviors of groups of mice, in an ethologically relevant environment, with minimal experimental intervention (Anpilov et al., 2020; Forkosh et al., 2019; Karamihalev et al., 2020; Shemesh et al., 2013). Adult male mice in groups of four were introduced into SBs (Figure 7D), under continuous video observation for 5 days and 6 nights (Figure 7E). The first 4 nights were used to establish individual and group baseline behaviors. Before the start of the dark phase on day 5, mice were administered either ketamine or saline. All mice were subsequently returned to a clean SB for response monitoring over the following 2 nights. This procedure was performed on an initial cohort of 64 mice (16 groups), allowing assessments of individual differences in ketamine response and establishment of an analysis pipeline for the SB data. A description of the pipeline is available in STAR Methods (Figures 7F, 7G, and S7A–S7D). Based on our partial least squares discriminant analysis (PLSDA) classifier, mice treated with ketamine spent more time exploring in an open area of the SB arena, using the distal feeder (feeding and drinking away from the nest), exploring in the central labyrinth, approaching others in the group, and engaged in more social behaviors with other members of their group, such as nose to nose contacts. On the other hand, these mice also spent less time around the walls and inside the main nest. These measures are all associated with anxiolytic behaviors in mice (Forkosh et al., 2019).

Furthermore, in order to determine whether pharmacological manipulation of KCNQ channels, following ketamine treatment, modulates the behavior of mice in an enriched group environment, a new cohort of 96 mice (24 groups) was introduced into the SBs. Baseline behaviors were assessed as above. On day 5, mice were administered 2 injections for a combination of either ketamine, retigabine (1 or 5 mg/kg), or a saline control (Figure 7H). An additional group of mice received a combination of ketamine and XE991 (1 mg/kg) (Figure S7E). The concentrations of retigabine and XE991 were based on our FST results (Figures 7C and S6I). Using a prediction algorithm for ketamine response (P-KET) developed and trained on our original cohort of mice (Figures 7E–7G), we monitored the behavior of all mice after treatment with saline or ketamine alone, or ketamine in combination with KCNQ modulators, for 2 additional nights. Consistent with the FST, we found a significant difference between saline- and ketamine-treated mice (Figure 7I). The combination with retigabine (1 mg/kg) produced a stronger effect in the SB, as compared with saline-treated mice (FC: 0.72, $p = 0.0005$). Again, ketamine-treated mice from this cohort displayed more social and anxiolytic behaviors. We did not find any significant differences between mice treated with a combination of ketamine and retigabine (5 mg/kg) or XE991, as compared with saline-treated controls (Figures 7I and S7E), suggesting that the combination of ketamine and retigabine at higher doses, or

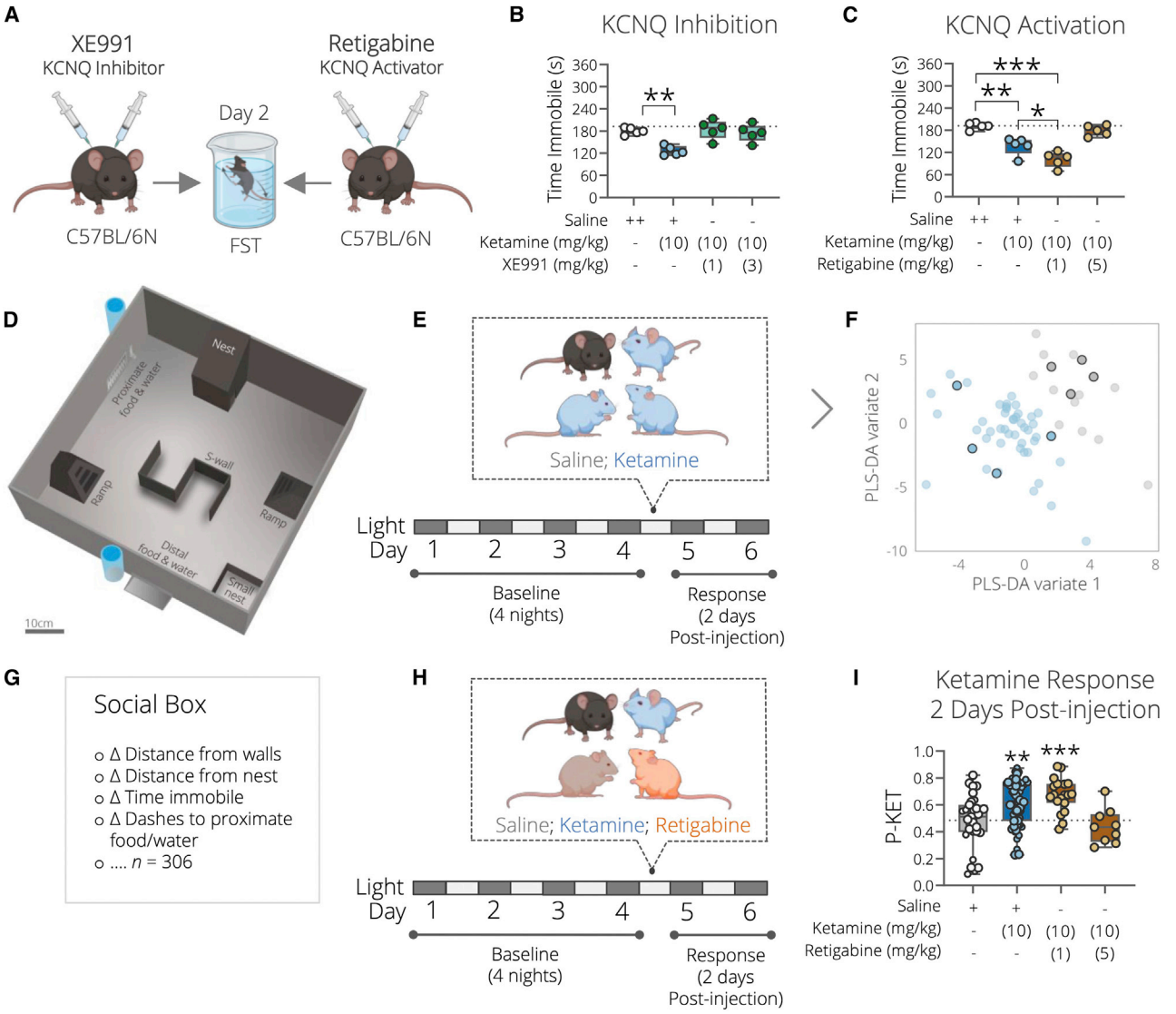


**Figure 7. Pharmacological manipulation of KCNQ modulates antidepressant-like behaviors**

(A) Schematic overview of pharmacological manipulation of KCNQ using XE991 or retigabine. Mice were treated with saline, ketamine (10 mg/kg/BW) alone, or a combination of ketamine with XE991 (1 and 3 mg/kg/BW) or retigabine (1 and 5 mg/kg/BW).

(B and C) Boxplots represent total immobile time (s) during the FST, 2 days after treatment. (n = 5, per condition) One-way ANOVA, corrected for multiple comparisons.

(D) The social box (SB) arena.

(E) Experimental timeline. On day 5, all mice were removed from the SBs and injected with ketamine (10 mg/kg/BW, n = 3 per group) or a saline solution (n = 1 per group). Following a recovery period, all mice were returned to a clean SB at the start of the dark phase for response monitoring.

(F and G) Behavioral outcomes from the SB were summarized as change from the mean over the baseline days and used as input for partial least squares discriminant analysis (PLS-DA).

(H) Experimental timeline. On day 5, mice were injected with saline, ketamine (10 mg/kg/BW), or ketamine in combination with retigabine (1 and 5 mg/kg/BW).

(I) Boxplots represent response to ketamine (P-KET) in the SB. Conditions: saline (gray), saline and ketamine (dark blue), ketamine and retigabine (dark orange). One-way ANOVA. Multiple testing was corrected using the Benjamini-Hochberg method. Data represented as mean ± SEM. ***p < 0.001, **p < 0.01, *p < 0.05. See also Figures S6 and S7.

inhibition of KCNQ channels, eliminates the antidepressant-like effects of ketamine in mice. These results are consistent with our FST results and suggest that ketamine and pharmacological manipulation of KCNQ channels modulate antidepressant-like behaviors in a semi-naturalistic living environment.

## Adjunctive treatment with retigabine augments the antidepressant-like effects of ketamine but not escitalopram in mice

Finally, we examined whether retigabine could increase the sustained antidepressant-like effects produced by a single injection

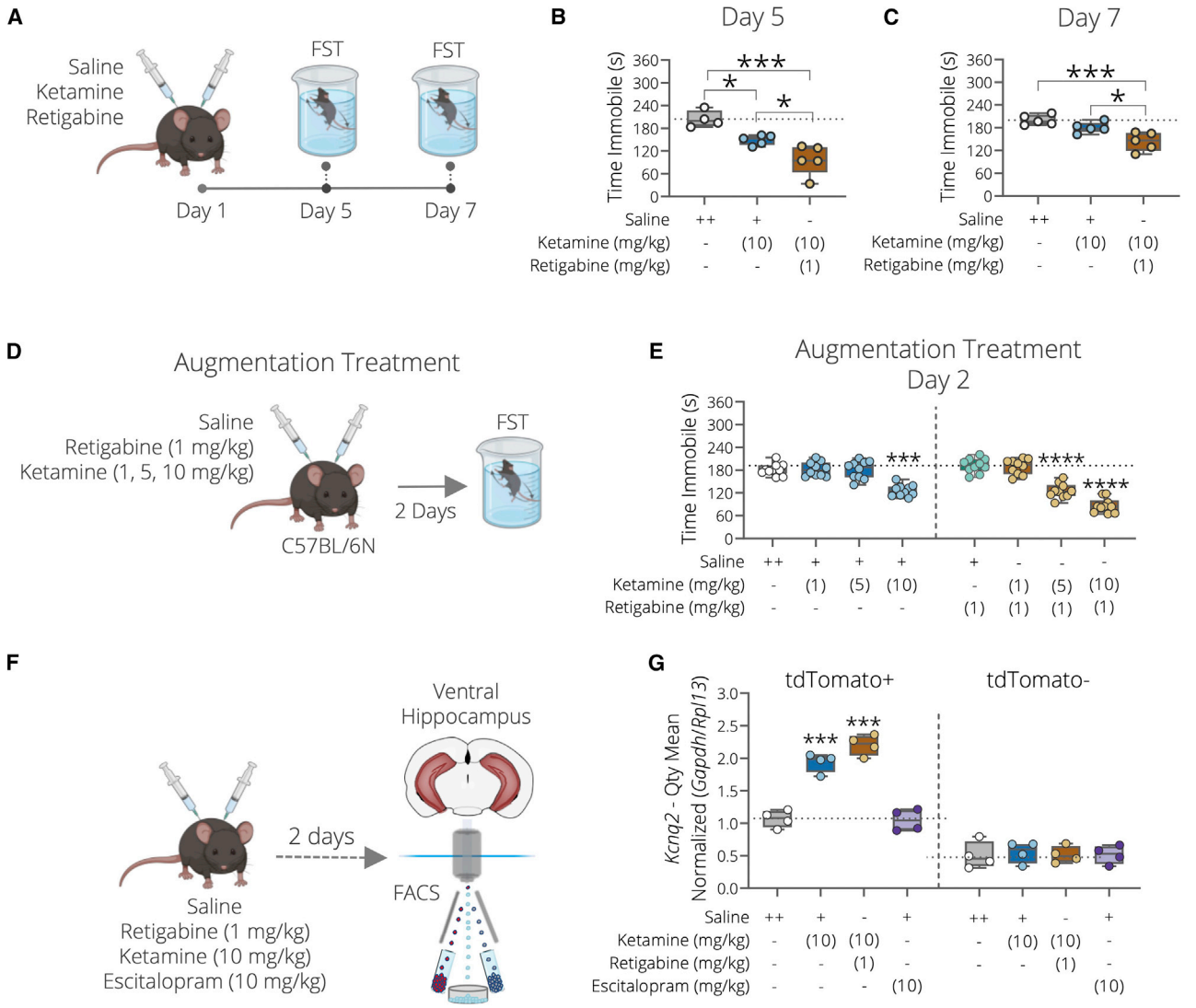


**Figure 8. Adjunctive treatment with retigabine augments the antidepressant-like effects of ketamine but not escitalopram**

(A) Overview of treatment. Each mouse was injected with saline or ketamine (10 mg/kg/BW) in the absence or in combination with retigabine (1 mg/kg/BW).

(B and C) Boxplots represent total immobile time (s) during the FST at days 5 and 7 post-injection. (n = 4, per condition).

(D) Schematic overview of pharmacological manipulation. Mice were injected with saline, ketamine (1, 5, or 10 mg/kg/BW) in the absence or in combination with retigabine (1 mg/kg/BW).

(E) Boxplots represent total immobile time (s) during the FST (2 days post-injection) (n = 10, per condition).

(F) Overview of treatment. Mice were injected with saline, escitalopram (10 mg/kg/BW), or ketamine (10 mg/kg/BW), in the absence or in combination with retigabine (1 mg/kg/BW).

(G) Boxplots represent qPCR mRNA levels of *Kcnq2* in tdTomato+ and tdTomato− cells. (n = 4, per condition). One-way ANOVA. Multiple testing was corrected using the Benjamini-Hochberg method. Data represented as mean ± SEM. ****p < 0.0001, ***p < 0.001, *p < 0.05. See also Figure S8.

of ketamine in mice. We treated a new cohort of mice with a single dose of saline, ketamine, or ketamine in combination with retigabine (1 mg/kg) and assessed antidepressant-like behaviors using the FST, 5 and 7 days post-injection (Figure 8A). Consistent with other studies, ketamine alone induced a significant decrease in immobility time during the FST that was sustained for several days post-injection (up to 5 days); however, these effects disappeared by day 7 (Figures 8B and 8C). Ketamine in combination with retigabine produced a significant decrease in immobility time during the FST at all time points (days 2, 5, and 7). Combined treatment had significantly stronger effects than ketamine alone at all time points (Figures 8B and 8C). Next, as a potential therapeutic strategy for MDD, we further investigated the synergistic effects of ketamine and retigabine by testing whether or not retigabine can increase the antidepressant-like effects produced by ketamine in mice. First, mice were treated with ketamine at sub-effective concentrations of 1 and 5 mg/kg/BW, an effective dose (10 mg/kg/BW), or a saline vehicle control and then assessed in the FST (Figure 8D). Consistent with our previous findings, we found a significant reduction

in immobility time in the FST only in mice treated with 10 mg/kg of ketamine, since lower doses failed to produce antidepressant-like effects (Figures 8E (left) and S8A). Remarkably, the combined treatment of ketamine with retigabine (1 mg/kg/BW) produced a significant reduction in immobility time during the FST in mice treated with both 5 and 10 mg/kg/BW of ketamine (Figure 8E (right) and S8A). Next, we tested whether retigabine can produce similar synergistic effects with traditional antidepressants. We selected escitalopram, a selective serotonin reuptake inhibitor and commonly prescribed antidepressant in humans that has shown efficacy in preclinical studies (Aguilar-Valles et al., 2021). Interestingly, we found that retigabine does not increase the antidepressant-like effects produced by escitalopram at any of the concentrations tested (Figures S8B and S8C). Lastly, using a new cohort of *Nex-Cre-Ai9* mice, we tested whether the adjunctive treatment of ketamine with retigabine, or escitalopram alone, can modify the expression of *Kcnq2* mRNA in FACS-sorted cells from the vHipp (Figure 8F). Consistent with our previous findings, we found a significant increase in *Kcnq2* mRNA in GLUT neurons (tdTomato+) of the vHipp, 2 days after treatment (Figure 8G, left). The combined treatment with retigabine led to a stronger increase in *Kcnq2* mRNA in GLUT neurons, as compared with ketamine alone (Figure 8G, left). We did not find any significant changes in *Kcnq2* mRNA expression after the treatment with escitalopram (Figure 8G, left) or with any of the medications tested in other cell types of the vHipp (tdTomato−) (Figure 8G, right). Interestingly, we found that none of the drugs tested increased the mRNA levels of *Kcnq2* in GLUT neurons (tdTomato+) or other cell types (tdTomato−) from the vHipp, 30 min after treatment (Figures S8D and S8E). These findings not only complement and verify our previous results but suggest that the adjunctive treatment with retigabine augments the antidepressant-like effects of ketamine at later time points and lower dosages. Moreover, our results imply that the synergistic effects of retigabine are specific to ketamine and not traditional antidepressants, suggesting that *Kcnq2* may play an important role in the sustained but not the immediate antidepressant effects of ketamine. In summary, adjunctive treatment with retigabine increases the sustained antidepressant-like effects of ketamine in mice, indicating the KCNQ channel as a promising target for MDD treatment.

## DISCUSSION

The discovery that a single sub-anesthetic dose of ketamine produces a rapid and sustained antidepressant response is one of the most important breakthroughs in psychiatry (Duman, 2018; Yang et al., 2018), yet the molecular mechanisms responsible for this remain unclear. Our study describes a previously unknown cell-type-specific molecular mechanism for the sustained effects of ketamine and provides new strategies for MDD treatment.

The vHipp is an important site for the sustained antidepressant effects of ketamine at the electrochemical, molecular, cellular, and circuit levels (Aguilar-Valles et al., 2021; Bagot et al., 2017; Carreno et al., 2016; Kim et al., 2021; Moda-Sava et al., 2019). However, due to methodological limitations, such as the absence of cell-type-specific information, some of the more elusive components of these mechanisms are still unidentified. Here, we used scRNA-seq to comprehensively catalog the transcriptome of thousands of single cells from the vHipp of male mice treated with ketamine and found cell-type-specific transcriptional signatures associated with its sustained antidepressant effects. Specifically, we identified a total of 263 DEGs in 7 of the 13 clusters. We identified the gene coding for the voltage-gated potassium channel, *Kcnq2*, as an important regulator of ketamine action in GLUT neurons of the vHipp. We validated these findings through a series of molecular, cellular, behavioral, pharmacological, and functional experiments using conditional reporter lines, FACS-sorted populations of GLUT neurons, *in vitro* assays in primary hippocampal neurons, electrophysiological recordings from *in vitro* cells and *ex vivo* acute slices, a validated mouse model to induce long-lasting depression- and anxiety-like endophenotypes, as well as a knockdown of *Kcnq2* in the vHipp.

*Kcnq2* and *Kcnq3* are the dominant variants in the central nervous system (Barrese et al., 2018) and in combination generate a signature M-current, which regulates the resting membrane potential and dampens repetitive neuronal firing, thus controlling neuronal excitability (Baculis et al., 2020). Whereas *Kncq2/3* overexpression is associated with increased regulation of repetitive neuronal firing due to excess stimuli or neurotransmitter release, low expression leads to neuronal hyperexcitability. In addition, loss of function has been linked with neurodevelopmental disorders, such as epilepsy (Dirkx et al., 2020). Recent studies have highlighted a potential role of the KCNQ channel in the pathophysiology of stress-related disorders. Stress exposure modulates the expression of *Kcnq2* and *Kcnq3* in the medial prefrontal cortex (Arnsten et al., 2019) and hippocampus of mice (Li et al., 2014). In the lateral habenula, dysregulation of KCNQ channels mediates hyperalgesia during alcohol withdrawal (Kang et al., 2019). In addition, *Kcnq3* is upregulated in the ventral tegmental area (VTA) of stress-resilient mice (Krishnan et al., 2007), and overexpression of *Kcnq3* in the VTA increases resilience to stress (Friedman et al., 2016). Interestingly, these are all important brain areas for control of rhythmic neuronal activity and synchronization, where KCNQ channels are concentrated (Cooper et al., 2001). Our results are consistent with these findings and provide further evidence that KCNQ channels are regulated by chronic stress and can regulate antidepressant-like behaviors in mice. Nevertheless, it is possible that the antidepressant effects of ketamine are non-mutually exclusive and likely complementary between these (and other brain) regions. Moreover, our findings point to a possible new role for *Kcnq2*, as ketamine did not affect *Kcnq3* mRNA either *in vitro* or *in vivo*. These differences could be explained by the distinct expression patterns shown by these two genes across regions of the mouse brain and within its cell types, suggesting that they may have specialized but complementary functions, where *Kcnq3* may have a role regulating active resilience mechanisms in multiple brain regions, whereas *Kcnq2* may play a more centralized role in the hippocampus modulating the sustained antidepressant effects of ketamine. In addition, our results offer a new level of resolution by identifying the specific cell types where these changes are taking place in the vHipp.

Previous studies have investigated the molecular mechanisms underlying both the fast and sustained antidepressant effects of

ketamine (Björkholm and Monteggia, 2016; Ma et al., 2017; Kim et al., 2021; Luo et al., 2021; Aguilar-Valles et al., 2021; Ho et al., 2019; Williams et al., 2018; Zanos and Gould, 2018). Although these studies have provided progress, the mechanisms of ketamine action are only partially understood. Among these known mechanisms, $Ca^{2+}$ signaling seems to be an upstream common denominator and might be an intermediate mechanism to induce fast-acting and sustained antidepressant effects (Figure 6E, left) (Ali et al., 2020; Kim et al., 2021). Our results build upon this and describe a complementary but previously unknown cell-type-specific mechanism for the sustained antidepressant effects of ketamine by *Kcnq2* via $Ca^{2+}$, CaM, CaN, and AKAP5 signaling (Figure 6E, right). More specifically, our results suggest that baseline KCNQ activity might be necessary for ketamine to exert its antidepressant actions. This is highlighted by our findings showing that ketamine elicits an acute antidepressant-like effect in the FST 30 min after ketamine injection, which can be disrupted by knockdown of KCNQ2 in the vHipp, as well as by systemic pharmacological modulation (inhibition or activation) of KCNQ channels *in vivo* (Figure S8A). Nevertheless, the mRNA levels of *Kcnq2* were only changed after 2 days of treatment and not 30 min post-injection (Figures S8D and S8E), suggesting that *Kcnq2* may play an important role in the sustained but not in the immediate antidepressant effects of ketamine. Based on our findings and the current literature, these fast (non-genomic) effects might not require direct transcriptional activation of *Kcnq2* mRNA but rather may act via direct activation of KCNQ2 proteins by CaM, a mechanism that was previously shown by Zhou and others (Zhou et al., 2016). In addition, our results show that ketamine treatment increases *Kcnq2* mRNA expression in GLUT neurons 2 days post-treatment *in vivo*, as well as after 1, 2, and up to 6 h *in vitro*. Based on our findings, and those of Zhang and Shapiro (2012), ketamine might elicit these effects via the CaM/CaN/AKAP5/NFAT transcription pathway, in GLUT neurons of the vHipp, to induce its sustained (genomic) antidepressant effects. This is the first study to show how ketamine regulates a sustained antidepressant response via the *Kcnq2* gene. In addition, our results highlight a critical role for L-type calcium channels, CaM (*Calm1* and *Calm2*), CaN, and AKAP5 (*Akap5*) for the transcriptional regulation of *Kcnq2* by ketamine treatment. Nevertheless, it is important to highlight the concentrations of ketamine and HNK that were used in our *in vitro* experiments, as this is still a debated topic (Aleksandrova et al., 2017). For example, some studies have suggested that low concentrations (~2 μM) should be used *in vitro* to mimic physiologically relevant concentrations in the brain (Zanos et al., 2016), whereas others using higher concentrations (~20 μM) have shown that ketamine and HNK can elicit relevant physiological, molecular, and electrophysiological effects *in vitro* (Kang et al., 2020; Lazarevic et al., 2021; Riggs et al., 2020; Suzuki et al., 2017). We chose a concentration of 10 μM following a viability assay to screen for the cytotoxic effects of ketamine and HNK at various concentrations and time points (Figures S3A–S3G) and after a comprehensive review of the literature.

From a translational and clinical perspective, our results provide additional evidence that pharmacological modulators of KCNQ channels can regulate antidepressant-like behaviors in mice. Previous studies have shown that chronic or repeated retigabine treatment (8-day intraperitoneal [i.p.] injections) normalizes neuronal hyperactivity and depressive-like behaviors in mice (Friedman et al., 2016). Others have shown that neuroinflammation produced by stress exposure leads to overproduction and release of inflammatory cytokines, which ultimately increases neuronal excitability. Notably, these effects can also be reversed by retigabine (Feng et al., 2019). In 2020, a small open-label clinical trial assessed the antidepressant effects of retigabine in MDD patients and showed that chronic treatment (10 weeks) was associated with an improvement in depressive symptoms (Tan et al., 2020). These findings were recently replicated in a small randomized placebo-controlled trial testing the effect of retigabine on clinical outcomes in depressed patients (Costi et al., 2021). In both studies, retigabine was well tolerated, and no serious adverse events were reported. However, none of these studies used ketamine or tested any potential interactions between retigabine and ketamine. Finally, in a recent study (Kim et al., 2021), the authors show that similar to ketamine, scopolamine can exert fast and sustained antidepressant-like effects in mice via BDNF-dependent MeCP2 phosphorylation. Interestingly, scopolamine is a muscarinic acetylcholine receptor (mAChR) antagonist, and the KCNQ channel, also known as "M" channel, is deactivated upon mAChR activation, hinting at the possibility that KCNQ channels might be playing a complementary role exerting the sustained antidepressant-like effects of other rapidly acting antidepressants, such scopolamine. Collectively, our findings not only demonstrate that a single dose of retigabine is sufficient to enhance the antidepressant-like effects of ketamine in mice, but further suggest that (1) it augments the sustained antidepressant-like effects of ketamine (up to 7 days), (2) it can induce similar antidepressant-like effects with lower (sub-effective) ketamine concentrations, which could potentially reduce some of the undesired side effects, and (3) the effects of KCNQ are ketamine specific, as they do not modulate a response to classical antidepressants. These findings have important clinical implications considering that both medications are currently FDA-approved agents and are already in widespread clinical use.

Our high-throughput, cell-type-specific findings for the role of *Kcnq2* in GLUT neurons of the vHipp provide a significant advancement to our understanding of the mechanisms underlying a sustained antidepressant effect of ketamine. Future studies should test the effects that the enantiomers and metabolites of ketamine have on KCNQ channels, as well as test whether inhibitors of NMDARs, AMPARs, the opiate system, and other potential signaling molecules affect *Kncq2* mRNA and protein expression. Our findings suggest that modulating KCNQ function, in combination with ketamine therapy, may be important in MDD treatment.

## STAR★METHODS

Detailed methods are provided in the online version of this paper and include the following:

- KEY RESOURCES TABLE
- RESOURCE AVAILABILITY
  - Lead contact

- Materials availability
- Data and software availability
- Data and code availability
- EXPERIMENTAL MODEL AND SUBJECT DETAILS
  - Animals and animal housing
- METHOD DETAILS
  - FST
  - scRNA-seq
  - Generation of Nex-Cre-Ai9 mice
  - FACS analysis of live cells
  - Reverse transcription and qRT-PCR
  - Primary cell culture
  - *Ex vivo* electrophysiological recordings
  - *In vitro* electrophysiological recordings
  - Cloning and validation of shRNA constructs
  - Virus production and stereotactic surgery
  - Chronic social defeat stress paradigm
  - Home cage activity
  - Plasma CORT measurements
  - Pharmacological experiments
  - The social box arenas
  - Characterization of the mouse behavioral response to ketamine
- QUANTIFICATION AND STATISTICAL ANALYSIS
  - scRNA-seq
  - Reverse transcription and qRT-PCR
  - *Ex Vivo* electrophysiological recordings
  - The social box arenas

## SUPPLEMENTAL INFORMATION

Supplemental information can be found online at https://doi.org/10.1016/j.neuron.2022.05.001.

## ACKNOWLEDGMENTS

We would like to thank A. Varga and his staff for their dedicated support with animal care; C. Kühne for her technical support; S. Unkmeir, S. Bauer, and the Genetically Engineered Mouse Models core unit for genotyping support; and J. Keverne for editorial support. J.P.L. holds fellowships from the European Molecular Biology Organization (EMBO-ALTF 650-2016), Alexander Von Humboldt Foundation, and the Canadian Biomarker Integration Network in Depression (CAN-BIND). J.D. is the incumbent of the Achar research fellow chair in electrophysiology. F.J.T. was supported by ExNet-0041-Phase2-3 (SyNergy-HMGU) and Incubator (ZT-I-0007 sparse2big) both through the Initiative and Network Fund of the Helmholtz Association and by the Chan Zuckerberg Foundation (2019-207271). A.C. is the incumbent of the Schwartz Family Professorial Chair in Neurobiology at WIS and the head of the MPS–WIS Laboratory for Experimental Neuropsychiatry and Behavioral Neurogenetics. This work is supported by the German Ministry of Science and Education (IMADAPT, FKZ: 01KU1901, J.M.D.). A.C. has research support from the Ruhman Family Laboratory for Research in the Neurobiology of Stress, Bruno and Simone Licht, the Perlman Family Foundation, the Adelis Foundation, and Sonia T. Marschak.

## AUTHOR CONTRIBUTIONS

Conceptualization and project administration, J.P.L. and A.C.; methodology, J.P.L., M.D.L., E.B., S.K., A.K., C.D.D., A.B., A.L.W.D., R.D.G., J.M.D., M.E., and J.D.; software, M.D.L., S.K., A.B., C.D.D., S.R., and F.J.T.; validation, J.P.L., E.B., S.K., A.K., H.Y., A.L.W.D., R.S., A.R., C.F., R.E.H., A.P., C.E., B.N., Y.Y., K.Y., M.H., B.H., D.H., B.S., R.D.G., C.W.T., J.M.D., M.E., and J.D.; formal analysis, J.P.L., M.D.L., S.K., A.K., H.Y., R.D.G., M.E., and J.D.; investigation, J.P.L., M.D.L., E.B., S.K., A.K., A.B., H.Y., R.S., A.R., C.F., R.E.H., A.P., C.E., M.H., B.H., R.D.G., and J.D.; resources, J.P.L., M.V.S., J.M.D., M.E., F.J.T., and A.C.; data curation, J.P.L., M.D.L., S.K., and S.R.; writing – original draft, J.P.L.; writing – review & editing, all authors; visualization, J.P.L., M.D.L., S.K., A.K., R.D.G., M.E., and J.D.; supervision, J.P.L., A.K., M.V.S., J.M.D., M.E., J.D., F.J.T., and A.C.; funding acquisition, A.C.

## DECLARATION OF INTERESTS

A.C. and J.P.L. are named on a patent pending for the combined use of retigabine (ezogabine) and ketamine to amplify antidepressant effects to treat depression and related conditions. F.J.T. reports receiving consulting fees from Roche Diagnostics GmbH and Cellarity Inc. and ownership interest in Cellarity, Inc. and Dermagnostix. All other authors declare no competing interests.

Received: July 27, 2021
Revised: March 1, 2022
Accepted: May 2, 2022
Published: May 31, 2022

## REFERENCES

Aguilar-Valles, A., De Gregorio, D., Matta-Camacho, E., Eslamizade, M.J., Khlaifia, A., Skaleka, A., Lopez-Canul, M., Torres-Berrio, A., Bermudez, S., Rurak, G.M., et al. (2021). Antidepressant actions of ketamine engage cell-specific translation via eIF4E. Nature *590*, 315–319.

Aleksandrova, L.R., Wang, Y.T., and Phillips, A.G. (2017). Hydroxynorketamine: implications for the NMDA receptor hypothesis of ketamine's antidepressant action. Chronic Stress (Thousand Oaks) *1*.

Ali, F., Gerhard, D.M., Sweasy, K., Pothula, S., Pittenger, C., Duman, R.S., and Kwan, A.C. (2020). Ketamine disinhibits dendrites and enhances calcium signals in prefrontal dendritic spines. Nat. Commun. *11*, 72.

Anpilov, S., Shemesh, Y., Eren, N., Harony-Nicolas, H., Benjamin, A., Dine, J., Oliveira, V.E.M., Forkosh, O., Karamihalev, S., Hüttl, R.E., et al. (2020). Wireless optogenetic stimulation of oxytocin neurons in a semi-natural setup dynamically elevates both pro-social and agonistic behaviors. Neuron *107*, 644–655.e7.

Arnsten, A.F.T., Jin, L.E., Gamo, N.J., Ramos, B., Paspalas, C.D., Morozov, Y.M., Kata, A., Bamford, N.S., Yeckel, M.F., Kaczmarek, L.K., and El-Hassar, L. (2019). Role of KCNQ potassium channels in stress-induced deficit of working memory. Neurobiol. Stress *11*, 100187.

Baculis, B.C., Zhang, J., and Chung, H.J. (2020). The role of Kv7 channels in neural plasticity and behavior. Front. Physiol. *11*, 568667.

Bagot, R.C., Cates, H.M., Purushothaman, I., Vialou, V., Heller, E.A., Yieh, L., LaBonté, B., Peña, C.J., Shen, L., Wittenberg, G.M., and Nestler, E.J. (2017). Ketamine and imipramine reverse transcriptional signatures of susceptibility and induce resilience-specific gene expression profiles. Biol. Psychiatry *81*, 285–295.

Barrese, V., Stott, J.B., and Greenwood, I.A. (2018). KCNQ-encoded potassium channels as therapeutic targets. Annu. Rev. Pharmacol. Toxicol. *58*, 625–648.

Björkholm, C., and Monteggia, L.M. (2016). BDNF - a key transducer of antidepressant effects. Neuropharmacology *102*, 72–79.

Buchsbaum, I.Y., Kielkowski, P., Giorgio, G., O'Neill, A.C., Di Giaimo, R., Kyrousi, C., Khattak, S., Sieber, S.A., Robertson, S.P., and Cappello, S. (2020). ECE2 regulates neurogenesis and neuronal migration during human cortical development. EMBO Rep. *21*, e48204.

Carreno, F.R., Donegan, J.J., Boley, A.M., Shah, A., DeGuzman, M., Frazer, A., and Lodge, D.J. (2016). Activation of a ventral hippocampus-medial prefrontal cortex pathway is both necessary and sufficient for an antidepressant response to ketamine. Mol. Psychiatry *21*, 1298–1308.

Cooper, E.C., Harrington, E., Jan, Y.N., and Jan, L.Y. (2001). M channel KCNQ2 subunits are localized to key sites for control of neuronal network oscillations and synchronization in mouse brain. J. Neurosci. *21*, 9529–9540.

Cooper, E.C., and Jan, L.Y. (2003). M-channels: neurological diseases, neuromodulation, and drug development. Arch. Neurol. *60*, 496–500.

Costi, S., Morris, L.S., Kirkwood, K.A., Hoch, M., Corniquel, M., Vo-Le, B., Iqbal, T., Chadha, N., Pizzagalli, D.A., Whitton, A., et al. (2021). Impact of the KCNQ2/3 channel opener ezogabine on reward circuit activity and clinical symptoms in depression: results from a randomized controlled trial. Am. J. Psychiatry *178*, 437–446.

Dirkx, N., Miceli, F., Taglialatela, M., and Weckhuysen, S. (2020). The role of Kv7.2 in neurodevelopment: insights and gaps in our understanding. Front. Physiol. *11*, 570588.

Duman, R.S. (2018). Ketamine and rapid-acting antidepressants: a new era in the battle against depression and suicide. F1000Res *7*.

Duman, R.S., Sanacora, G., and Krystal, J.H. (2019). Altered connectivity in depression: GABA and glutamate neurotransmitter deficits and reversal by novel treatments. Neuron *102*, 75–90.

Feng, M., Crowley, N.A., Patel, A., Guo, Y., Bugni, S.E., and Luscher, B. (2019). Reversal of a treatment-resistant, depression-related brain state with the Kv7 channel opener retigabine. Neuroscience *406*, 109–125.

Ficek, J., Zygmunt, M., Piechota, M., Hoinkis, D., Rodriguez Parkitna, J., Przewlocki, R., and Korostynski, M. (2016). Molecular profile of dissociative drug ketamine in relation to its rapid antidepressant action. BMC Genomics *17*, 362.

Fiori, L.M., Kos, A., Lin, R., Théroux, J.F., Lopez, J.P., Kühne, C., Eggert, C., Holzapfel, M., Huettl, R.E., Mechawar, N., et al. (2021). miR-323a regulates ERBB4 and is involved in depression. Mol. Psychiatry *26*, 4191–4204.

Forkosh, O., Karamihalev, S., Roeh, S., Alon, U., Anpilov, S., Touma, C., Nussbaumer, M., Flachskamm, C., Kaplick, P.M., Shemesh, Y., and Chen, A. (2019). Identity domains capture individual differences from across the behavioral repertoire. Nat. Neurosci. *22*, 2023–2028.

Friedman, A.K., Juarez, B., Ku, S.M., Zhang, H., Calizo, R.C., Walsh, J.J., Chaudhury, D., Zhang, S., Hawkins, A., Dietz, D.M., et al. (2016). KCNQ channel openers reverse depressive symptoms via an active resilience mechanism. Nat. Commun. *7*, 11671.

Gastaldon, C., Papola, D., Ostuzzi, G., and Barbui, C. (2019). Esketamine for treatment resistant depression: a trick of smoke and mirrors? Epidemiol. Psychiatr. Sci. *29*, e79.

Girardot, C., Scholtalbers, J., Sauer, S., Su, S.Y., and Furlong, E.E. (2016). Je, a versatile suite to handle multiplexed NGS libraries with unique molecular identifiers. BMC Bioinformatics *17*, 419.

Goebbels, S., Bormuth, I., Bode, U., Hermanson, O., Schwab, M.H., and Nave, K.A. (2006). Genetic targeting of principal neurons in neocortex and hippocampus of NEX-Cre mice. Genesis *44*, 611–621.

Greene, D.L., Kang, S., and Hoshi, N. (2017). XE991 and linopirdine are state-dependent inhibitors for Kv7/KCNQ channels that favor activated single subunits. J. Pharmacol. Exp. Ther. *362*, 177–185.

Gururajan, A., Kos, A., and Lopez, J.P. (2018). Preclinical stress research: where are we headed? An early career investigator's perspective. Stress *21*, 384–388.

Hafemeister, C., and Satija, R. (2019). Normalization and variance stabilization of single-cell RNA-seq data using regularized negative binomial regression. Genome Biol. *20*, 296.

Hartmann, J., Dedic, N., Pöhlmann, M.L., Häusl, A., Karst, H., Engelhardt, C., Westerholz, S., Wagner, K.V., Labermaier, C., Hoeijmakers, L., et al. (2017). Forebrain glutamatergic, but not GABAergic, neurons mediate anxiogenic effects of the glucocorticoid receptor. Mol. Psychiatry *22*, 466–475.

Ho, M.F., Zhang, C., Zhang, L., Li, H., and Weinshilboum, R.M. (2019). Ketamine and active ketamine metabolites regulate STAT3 and the type I interferon pathway in human microglia: molecular mechanisms linked to the antidepressant effects of ketamine. Front. Pharmacol. *10*, 1302.

Ionescu, D.F., Felicione, J.M., Gosai, A., Cusin, C., Shin, P., Shapero, B.G., and Deckersbach, T. (2018). Ketamine-associated brain changes: a review of the neuroimaging literature. Harv. Rev. Psychiatry *26*, 320–339.

Jentsch, T.J. (2000). Neuronal KCNQ potassium channels: physiology and role in disease. Nat. Rev. Neurosci. *1*, 21–30.

Kalappa, B.I., Soh, H., Duignan, K.M., Furuya, T., Edwards, S., Tzingounis, A.V., and Tzounopoulos, T. (2015). Potent KCNQ2/3-specific channel activator suppresses in vivo epileptic activity and prevents the development of tinnitus. J. Neurosci. *35*, 8829–8842.

Kang, H., Park, P., Han, M., Tidball, P., Georgiou, J., Bortolotto, Z.A., Lodge, D., Kaang, B.K., and Collingridge, G.L. (2020). (2S,6S)- and (2R,6R)-hydroxynorketamine inhibit the induction of NMDA receptor-dependent LTP at hippocampal CA1 synapses in mice. Brain Neurosci. Adv. *4*.

Kang, S., Li, J., Zuo, W., Chen, P., Gregor, D., Fu, R., Han, X., Bekker, A., and Ye, J.H. (2019). Downregulation of M-channels in lateral habenula mediates hyperalgesia during alcohol withdrawal in rats. Sci. Rep. *9*, 2714.

Karamihalev, S., Brivio, E., Flachskamm, C., Stoffel, R., Schmidt, M.V., and Chen, A. (2020). Social dominance mediates behavioral adaptation to chronic stress in a sex-specific manner. eLife *9*.

Kim, J.W., Autry, A.E., Na, E.S., Adachi, M., Björkholm, C., Kavalali, E.T., and Monteggia, L.M. (2021). Sustained effects of rapidly acting antidepressants require BDNF-dependent MeCP2 phosphorylation. Nat. Neurosci. *24*, 1100–1109.

Kraguljac, N.V., Frölich, M.A., Tran, S., White, D.M., Nichols, N., Barton-McArdle, A., Reid, M.A., Bolding, M.S., and Lahti, A.C. (2017). Ketamine modulates hippocampal neurochemistry and functional connectivity: a combined magnetic resonance spectroscopy and resting-state fMRI study in healthy volunteers. Mol. Psychiatry *22*, 562–569.

Krishnan, V., Han, M.H., Graham, D.L., Berton, O., Renthal, W., Russo, S.J., Laplant, Q., Graham, A., Lutter, M., Lagace, D.C., et al. (2007). Molecular adaptations underlying susceptibility and resistance to social defeat in brain reward regions. Cell *131*, 391–404.

Krystal, J.H., Abdallah, C.G., Sanacora, G., Charney, D.S., and Duman, R.S. (2019). Ketamine: a paradigm shift for depression research and treatment. Neuron *101*, 774–778.

Lazarevic, V., Yang, Y., Flais, I., and Svenningsson, P. (2021). Ketamine decreases neuronally released glutamate via retrograde stimulation of presynaptic adenosine A1 receptors. Mol. Psychiatry *26*, 7425–7435.

Lein, E.S., Hawrylycz, M.J., Ao, N., Ayres, M., Bensinger, A., Bernard, A., Boe, A.F., Boguski, M.S., Brockway, K.S., Byrnes, E.J., et al. (2007). Genome-wide atlas of gene expression in the adult mouse brain. Nature *445*, 168–176.

Li, C., Huang, P., Lu, Q., Zhou, M., Guo, L., and Xu, X. (2014). KCNQ/Kv7 channel activator flupirtine protects against acute stress-induced impairments of spatial memory retrieval and hippocampal LTP in rats. Neuroscience *280*, 19–30.

Li, N., Lee, B., Liu, R.J., Banasr, M., Dwyer, J.M., Iwata, M., Li, X.Y., Aghajanian, G., and Duman, R.S. (2010). mTOR-dependent synapse formation underlies the rapid antidepressant effects of NMDA antagonists. Science *329*, 959–964.

Lopez, J.P., Brivio, E., Santambrogio, A., De Donno, C., Kos, A., Peters, M., Rost, N., Czamara, D., Brückl, T.M., Roeh, S., et al. (2021). Single-cell molecular profiling of all three components of the HPA axis reveals adrenal ABCB1 as a regulator of stress adaptation. Sci. Adv. *7*.

Luecken, M.D., and Theis, F.J. (2019). Current best practices in single-cell RNA-seq analysis: a tutorial. Mol. Syst. Biol. *15*, e8746.

Lun, A.T., Bach, K., and Marioni, J.C. (2016). Pooling across cells to normalize single-cell RNA sequencing data with many zero counts. Genome Biol. *17*, 75.

Luo, Y., Yu, Y., Zhang, M., He, H., and Fan, N. (2021). Chronic administration of ketamine induces cognitive deterioration by restraining synaptic signaling. Mol. Psychiatry *26*, 4702–4718.

Lur, G., Fariborzi, M., and Higley, M.J. (2019). Ketamine disrupts neuromodulatory control of glutamatergic synaptic transmission. PLoS One *14*, e0213721.

Ma, Z., Zang, T., Birnbaum, S.G., Wang, Z., Johnson, J.E., Zhang, C.L., and Parada, L.F. (2017). TrkB dependent adult hippocampal progenitor differentiation mediates sustained ketamine antidepressant response. Nat. Commun. *8*, 1668.

Madisen, L., Zwingman, T.A., Sunkin, S.M., Oh, S.W., Zariwala, H.A., Gu, H., Ng, L.L., Palmiter, R.D., Hawrylycz, M.J., Jones, A.R., et al. (2010). A robust and high-throughput Cre reporting and characterization system for the whole mouse brain. Nat. Neurosci. *13*, 133–140.

Martin, M. (2011). Cutadapt removes adapter sequences from high-throughput sequencing reads. EMBnet J. *17*.

Mastrodonato, A., Martinez, R., Pavlova, I.P., LaGamma, C.T., Brachman, R.A., Robison, A.J., and Denny, C.A. (2018). Ventral CA3 activation mediates prophylactic ketamine efficacy against stress-induced depressive-like behavior. Biol. Psychiatry *84*, 846–856.

Mathis, A., Mamidanna, P., Cury, K.M., Abe, T., Murthy, V.N., Mathis, M.W., and Bethge, M. (2018). DeepLabCut: markerless pose estimation of user-defined body parts with deep learning. Nat. Neurosci. *21*, 1281–1289.

Mayer, C., Hafemeister, C., Bandler, R.C., Machold, R., Batista Brito, R., Jaglin, X., Allaway, K., Butler, A., Fishell, G., and Satija, R. (2018). Developmental diversification of cortical inhibitory interneurons. Nature *555*, 457–462.

Moda-Sava, R.N., Murdock, M.H., Parekh, P.K., Fetcho, R.N., Huang, B.S., Huynh, T.N., Witztum, J., Shaver, D.C., Rosenthal, D.L., Alway, E.J., et al. (2019). Sustained rescue of prefrontal circuit dysfunction by antidepressant-induced spine formation. Science *364*.

Nasca, C., Zelli, D., Bigio, B., Piccinin, S., Scaccianoce, S., Nisticò, R., and McEwen, B.S. (2015). Stress dynamically regulates behavior and glutamatergic gene expression in hippocampus by opening a window of epigenetic plasticity. Proc. Natl. Acad. Sci. USA *112*, 14960–14965.

Nigro, M.J., Mateos-Aparicio, P., and Storm, J.F. (2014). Expression and functional roles of Kv7/KCNQ/M-channels in rat medial entorhinal cortex layer II stellate cells. J. Neurosci. *34*, 6807–6812.

Patro, R., Duggal, G., Love, M.I., Irizarry, R.A., and Kingsford, C. (2017). Salmon provides fast and bias-aware quantification of transcript expression. Nat. Methods *14*, 417–419.

Pothula, S., Kato, T., Liu, R.J., Wu, M., Gerhard, D., Shinohara, R., Sliby, A.N., Chowdhury, G.M.I., Behar, K.L., Sanacora, G., et al. (2021). Cell-type specific modulation of NMDA receptors triggers antidepressant actions. Mol. Psychiatry *26*, 5097–5111.

Riggs, L.M., Aracava, Y., Zanos, P., Fischell, J., Albuquerque, E.X., Pereira, E.F.R., Thompson, S.M., and Gould, T.D. (2020). (2R,6R)-hydroxynorketamine rapidly potentiates hippocampal glutamatergic transmission through a synapse-specific presynaptic mechanism. Neuropsychopharmacology *45*, 426–436.

Ritchie, M.E., Phipson, B., Wu, D., Hu, Y., Law, C.W., Shi, W., and Smyth, G.K. (2015). limma powers differential expression analyses for RNA-sequencing and microarray studies. Nucleic Acids Res. *43*, e47.

Rohart, F., Gautier, B., Singh, A., and Lê Cao, K.A. (2017). mixOmics: an R package for 'omics feature selection and multiple data integration. PLoS Comput. Biol. *13*, e1005752.

Schneider, C., Rasband, W., and Eliceiri, K. (2012). NIH Image to ImageJ: 25 years of image analysis. Nat. Methods *9*, 671–675. https://doi.org/10.1038/nmeth.2089.

Schraut, K.G., Kalnytska, O., Lamp, D., Jastroch, M., Eder, M., Hausch, F., Gassen, N.C., Moore, S., Nagaraj, N., Lopez, J.P., et al. (2021). Loss of the psychiatric risk factor SLC6A15 is associated with increased metabolic functions in primary hippocampal neurons. Eur. J. Neurosci. *53*, 390–401.

Shemesh Y., Forkosh O., Chen A. and Schneidman E. (2020). Mouse tracking. Bio-protocol. https://bio-protocol.org/prep207

Shemesh, Y., Sztainberg, Y., Forkosh, O., Shlapobersky, T., Chen, A., and Schneidman, E. (2013). High-order social interactions in groups of mice. eLife *2*, e00759.

Simon, R.A. (2019). FastQC: a quality control tool for high throughput sequence data. https://www.bioinformatics.babraham.ac.uk/projects/fastqc/

Smith, T., Heger, A., and Sudbery, I. (2017). UMI-tools: modeling sequencing errors in unique molecular identifiers to improve quantification accuracy. Genome Res. *27*, 491–499.

Suzuki, K., Nosyreva, E., Hunt, K.W., Kavalali, E.T., and Monteggia, L.M. (2017). Effects of a ketamine metabolite on synaptic NMDAR function. Nature *546*, E1–E3.

Tan, A., Costi, S., Morris, L.S., Van Dam, N.T., Kautz, M., Whitton, A.E., Friedman, A.K., Collins, K.A., Ahle, G., Chadha, N., et al. (2020). Effects of the KCNQ channel opener ezogabine on functional connectivity of the ventral striatum and clinical symptoms in patients with major depressive disorder. Mol. Psychiatry *25*, 1323–1333.

Tasic, B., Yao, Z., Graybuck, L.T., Smith, K.A., Nguyen, T.N., Bertagnolli, D., Goldy, J., Garren, E., Economo, M.N., Viswanathan, S., et al. (2018). Shared and distinct transcriptomic cell types across neocortical areas. Nature *563*, 72–78.

Valdor, M., Wagner, A., Röhrs, V., Berg, J., Fechner, H., Schröder, W., Tzschentke, T.M., Bahrenberg, G., Christoph, T., and Kurreck, J. (2018). RNA interference-based functional knockdown of the voltage-gated potassium channel Kv7.2 in dorsal root ganglion neurons after in vitro and in vivo gene transfer by adeno-associated virus vectors. Mol. Pain *14*.

Williams, N.R., Heifets, B.D., Blasey, C., Sudheimer, K., Pannu, J., Pankow, H., Hawkins, J., Birnbaum, J., Lyons, D.M., Rodriguez, C.I., and Schatzberg, A.F. (2018). Attenuation of antidepressant effects of ketamine by opioid receptor antagonism. Am. J. Psychiatry *175*, 1205–1215.

Wolf, F.A., Angerer, P., and Theis, F.J. (2018). SCANPY: large-scale single-cell gene expression data analysis. Genome Biol. *19*, 15.

Xie, Z., Bailey, A., Kuleshov, M.V., Clarke, D.J.B., Evangelista, J.E., Jenkins, S.L., Lachmann, A., Wojciechowicz, M.L., Kropiwnicki, E., Jagodnik, K.M., et al. (2021). Gene set knowledge discovery with Enrichr. Curr. Protoc. *1*, e90.

Yang, Y., Cui, Y., Sang, K., Dong, Y., Ni, Z., Ma, S., and Hu, H. (2018). Ketamine blocks bursting in the lateral habenula to rapidly relieve depression. Nature *554*, 317–322.

Yankelevitch-Yahav, R., Franko, M., Huly, A., and Doron, R. (2015). The forced swim test as a model of depressive-like behavior. J. Vis. Exp. *97*.

Zanos, P., and Gould, T.D. (2018). Mechanisms of ketamine action as an antidepressant. Mol. Psychiatry *23*, 801–811.

Zanos, P., Moaddel, R., Morris, P.J., Georgiou, P., Fischell, J., Elmer, G.I., Alkondon, M., Yuan, P., Pribut, H.J., Singh, N.S., et al. (2016). NMDAR inhibition-independent antidepressant actions of ketamine metabolites. Nature *533*, 481–486.

Zeisel, A., Hochgerner, H., Lönnerberg, P., Johnsson, A., Memic, F., van der Zwan, J., Häring, M., Braun, E., Borm, L.E., La Manno, G., et al. (2018). Molecular architecture of the mouse nervous system. Cell *174*, 999–1014.e22.

Zhang, J., and Shapiro, M.S. (2012). Activity-dependent transcriptional regulation of M-Type (Kv7) K(+) channels by AKAP79/150-mediated NFAT actions. Neuron *76*, 1133–1146.

Zhou, X., Zhuang, F., Li, H., Zheng, K., Hong, Z., Feng, W., Zhou, W., and Chen, J. (2016). Calmodulin regulates KCNQ2 function in epilepsy. Am. J. Transl. Res. *8*, 5610–5618.

## STAR★METHODS

### KEY RESOURCES TABLE

| REAGENT or RESOURCE | SOURCE | IDENTIFIER |
|---|---|---|
| **Antibodies** | | |
| CORT Double Antibody 125I RIA Kit | MP Biomedicals Inc. | Cat # RIA-1364 |
| **Bacterial and virus strains** | | |
| pAAV-H1-Ctrl-shRNA-EF1a-eGFP | This Manuscript | N/A |
| pAAV-H1-KCNQ-shRNA1-EF1a-eGFP | This Manuscript | N/A |
| pAAV-H1-KCNQ-shRNA2-EF1a-eGFP | This Manuscript | N/A |
| **Chemicals, peptides, and recombinant proteins** | | |
| (*R*,*S*)-Ketamine Hydrochloride – Ketaset | Zoetis | N/A |
| (2R,6R)-HNK | Sigma | Cat # SML1873 |
| Nifedipine | Tocris | Cat # 1075 |
| W-7 Hydrochloride | Tocris, | Cat # 0369 |
| Cyclosporine-A | Tocris | Cat # 1101 |
| XE991 | Alomone labs | Cat # X-100 |
| Retigabine | Alomone labs | Cat # R-100 |
| **Critical commercial assays** | | |
| Papain Dissociation System | Worthington BC | Cat # LK003163 |
| MiRNeasy Mini Kit | Qiagen | Cat # / ID: 217004 |
| High-Capacity cDNA Reverse Transcription Kit | Thermo Fisher | Cat # 4374966 |
| iCELL8 Single-Cell System | Takara Bio | Cat # 640188 |
| Qubit dsDNA HS Assay Kit | Thermo Fisher | Cat # Q32855 |
| Qubit dsDNA BR Assay Kit | Thermo Fisher | Cat # Q10211 |
| QuantiFast SYBR Green PCR Kit | Qiagen | Cat # Q204057 |
| **Deposited data** | | |
| Code to Replicate ScRNA-Seq Analyses | This Manuscript | https://github.com/theislab/sc_ketamine_analysis |
| Mouse Genome Assembly (mm10) | National Center for Biotechnology Information (NCBI) | https://www.ncbi.nlm.nih.gov/assembly/GCF_000001635.20/ |
| Allen Brain Atlas: Mouse Brain | Lein et al. (2007) | https://mouse.brain-map.org/ |
| Allen Brain Map: Cell Types Database: RNA-Seq Data | Tasic et al. (2018) | https://portal.brain-map.org/atlases-and-data/rnaseq |
| Mouse Brain Atlas | Zeisel et al. (2018) | http://mousebrain.org/ |
| **Experimental models: Cell lines** | | |
| Primary Hippocampal Neurons | This Manuscript | N/A |
| Mouse Neuroblastoma neuro2a (N2a) Cells | This Manuscript | N/A |
| **Experimental models: Organisms/strains** | | |
| Mouse: C57BL/6N Male Mice | MPI Biochemistry (Germany) | N/A |
| Mouse: CD-1 (ICR) Male Mice | Harlan Laboratories (Israel) | N/A |
| Mouse: *Nex-Cre-Ai9* Male Mice | MPI Psychiatry (Germany) | N/A |
| **Software and algorithms** | | |
| QuantStudio Real-Time PCR Software | Thermo Fisher | https://www.thermofisher.com/de/de/home/global/forms/life-science/quantstudio-6-7-flex-software.html |
| *Jemultiplexer* version 1.0.6 | Girardot et al. (2016) | https://gbcs.embl.de/portal/tiki-index.php?page=Jemultiplexer |
| *Cutadapt* version 1.11 | Martin (2011) | https://cutadapt.readthedocs.io/en/stable/ |
| *UMI-Tools* version 0.5.4 | Smith et al. (2017) | https://github.com/CGATOxford/UMI-tools |

(*Continued on next page*)

*Continued*

| REAGENT or RESOURCE | SOURCE | IDENTIFIER |
|---|---|---|
| *Salmon* version 0.8.2 | Patro et al. (2017) | https://github.com/COMBINE-lab/salmon/releases |
| *Scanpy* version 1.5.1 | Wolf et al. (2018) | https://scanpy.readthedocs.io/en/stable/installation.html |
| Limma Package version 3.46.0 | Ritchie et al. (2015) | https://rdrr.io/bioc/limma/ |
| MATLAB | Mathworks | https://www.mathworks.com/products/matlab.html |
| DeepLabCut v.2.1.10) | Mathis et al. (2018) | https://github.com/DeepLabCut |
| *mixOmics* Package in R | Rohart et al. (2017) | https://www.bioconductor.org/packages/release/bioc/html/mixOmics.html |
| Prism v.8 | GraphPad | https://www.graphpad.com/scientific-software/prism/ |
| Bioinformatics & Evolutionary Genomics: Venn Diagrams | VIB / UGent | http://bioinformatics.psb.ugent.be/webtools/Venn/ |
| Enrichr: Pathway Analyses | Xie et al. (2021) | https://maayanlab.cloud/Enrichr/ |
| BioRender | BioRender | https://biorender.com/ |
| ImageJ | Schneider et al. (2012) | https://imagej.nih.gov/ij/ |

## RESOURCE AVAILABILITY

### Lead contact

Further information and requests for resources and reagents should be directed to and will be fulfilled by the lead contact, Alon Chen (alon_chen@psych.mpg.de or alon.chen@weizmann.ac.il).

### Materials availability

This study did not generate new unique reagents and all materials are available commercially.

### Data and software availability

This study did not generate new unique reagents and all materials are available commercially.

### Data and code availability

All data needed to evaluate the conclusions in the paper are present in the paper and/or the Supplementary Materials. Additional data related to this study may be obtained from the lead contact upon request. The code to replicate the analyses of our single-cell data can be found here: https://github.com/theislab/sc_ketamine_analysis

## EXPERIMENTAL MODEL AND SUBJECT DETAILS

### Animals and animal housing

All experiments were performed in accordance with the European Communities' Council Directive 2010/63/EU. All protocols were approved by the Ethics Committee for the Care and Use of Laboratory Animals of the government of Upper Bavaria, Germany and by the Institutional Animal Care and Use Committee (IACUC) of the Weizmann Institute of Science (Rehovot, Israel). CD-1 (ICR) and C57BL/6N male mice aged between 7 and 11 weeks old were used for all experiments. Mice were bred in the animal facility of the Max Planck Institute of Biochemistry (Martinsried, Germany). Mice were kept in individually ventilated cages (IVC; 30 cm × 16 cm × 16 cm; 501 $cm^2$), serviced by a central airflow system (Tecniplast, IVC Green Line – GM500), according to institutional guidelines. IVCs had sufficient bedding and nesting material as well as a wooden tunnel for environmental enrichment. Animals were maintained under a pathogen-free, temperature-controlled environment (23°C ± 1°C) and constant humidity (55% ± 10%) on a 12-h light-dark cycle (lights on at 7 a.m.) with food and water provided *ad libitum*, at the Max Planck Institute of Psychiatry (Munich, Germany). ***Note***: for all mouse experiments in this paper using ketamine treatment, we used 10 mg/kg/body weight (R,S)-ketamine intraperitoneally (i.p.) unless otherwise stated.

## METHOD DETAILS

### FST

Mice were placed in a 2-L glass beaker filled with 1.5 L of water at room-temperature (23°C ± 1°C) to a height of 14 cm so that the mouse could neither escape nor touch the bottom. The test lasted 6 min and was later analyzed by an experienced experimenter, blind to the experimental group. Time spent immobile and time spent struggling during the test were scored.

## scRNA-seq

### *Tissue dissociation*

Single-cell procedures were performed as previously described (Lopez et al., 2021). Mice were anesthetized lethally using isoflurane and perfused with cold PBS in order to get rid of undesired blood cells in target tissues. Brains were quickly dissected and immediately transferred to ice-cold oxygenated artificial cerebral spinal fluid (aCSF) and kept in the same solution during dissection and dissociation. The aCSF was oxygenated throughout the experiment with a mixture of 5% $CO_2$ in $O_2$. Sectioning of the brain was performed using a VT1200/S Leica vibratome. A 1000-μm thick slice (approximately −2.46-mm bregma to −3.52-mm bregma) was obtained from each brain and the vHipp was manually dissected under a stereo microscope (M205C, Leica, Wetzlar, Germany). The vHipp was dissociated using the Papain dissociation system (Worthington) for 35 min at 37°C in a shaking water bath, following the manufacturer's instructions. All cell suspensions were filtered with 30 μm filters (Partec) and kept in cold aCSF.

### *Cell capture, library preparation, and high-throughput sequencing*

Single cells were resuspended in ice-cold aCSF and prepared for single-cell labeling and capture using the iCELL8 Single-Cell System (Takara Bio, Kyoto), according to the manufacturer's recommendations. Cells were stained with DAPI (for live cells) and propidium iodide (for dead cells) for 10 min and dispensed in the loading plate. Each iCell8 chip was loaded with cells from two different mice (ketamine and saline treated). Following microfluidic separation, iCell8 chips were imaged using the built-in fluorescence microscope, snap-frozen using dry ice and stored at −80°C until library preparation. Based on fluorescence labeling, only wells containing live single cells were selected for library preparation. All wells containing dead cells or multiplets were excluded. Libraries were prepared according to the manufacturers' guidelines using the iCell8 Chip and Reagent Kit, in-chip RT-PCR amplification chemistry (Wafergen, Takara Bio), Nextera XT DNA Library Preparation Kit, and Nextera XT Index Kit (Illumina). Libraries were assessed using a High Sensitivity DNA Analysis Kit for the 2100 Bioanalyzer (Agilent, Santa Clara, CA, United States of America) and KAPA Library Quantification kit for Illumina (KAPA Biosystems), and sequencing was performed paired-end with 26-nt/100nt configuration on an Illumina HiSeq4000 system at the Helmholtz Zentrum Sequencing Core Facility (Munich, DE).

## Generation of Nex-Cre-Ai9 mice

Conditional transgenic mice expressing tdTomato in glutamatergic neurons of the forebrain (Nex-Cre-Ai9) were generated by crossing homozygous Nex-Cre mice (Goebbels et al., 2006) with homozygous Ai9 mice [Gt(ROSA)26Sor$^{tm9(CAG-tdTomato)Hze}$] (Madisen et al., 2010). Most glutamatergic neurons of the forebrain in *Nex-Cre-Ai9* mice, including the hippocampus, are fluorescently labeled by tdTomato, except for neurons in the dentate gyrus where *Neurod6*, the promoter used to target glutamatergic neurons driving Cre expression, is not expressed (Figure S2A) (Hartmann et al., 2017).

## FACS analysis of live cells

For FACS analysis, single-cell suspensions from the vHipp of mice treated with ketamine or a saline control were prepared as described earlier (see *tissue dissociation*). Four samples per treatments were analyzed as biological replicates. The procedure followed was described previously (Buchsbaum et al., 2020). FACS analysis was performed with a FACS Melody (BD) in BD FACS Flow TM medium, with a nozzle diameter of 100 μm. Debris and cell aggregates were gated out by forward scatter (FSC)-side scatter (SSC). Single cells were gated by FSC-W/FSC-A. Gating strategies for *Td*Tomato+ cells were selected using single-cell suspensions of vHipp from wild-type C57BL/6N mice. Examples of the gating strategy are shown in Figure S2.

## Reverse transcription and qRT-PCR

Messenger RNA (mRNA) samples were extracted using the miRNeasy kit according to the manufacturer's instructions (Qiagen). Quantification of mRNA levels (bulk) was carried out using qRT PCR. Total RNA was reverse transcribed using the High-Capacity cDNA Reverse Transcription Kit (Applied Biosystems, Waltham, MA, United States of America). The following primers were used:

| Primer Name | Sequence |
|---|---|
| *C1qc*_Fwd | GTGCACCTGAACCTCAACCT |
| *C1qc*_Rev | CGGGAAACAGTAGGAAACCA |
| *Clasp1*_Fwd | ACAGCTCTTTGCGTGGAGTT |
| *Clasp1*_Rev | GCCATCCTGCCTCCTTCTAT |
| *Cldn5*_Fwd | CTGGACCACAACATCGTGAC |
| *Cldn5*_Rev | GCCGGTCAAGGTAACAAAGA |
| *E2f1*_Fwd | CAACTGCAGGAGAGTGAGCA |
| *E2f1*_Rev | CCATCTGTTCTGCAGGGTCT |
| *Gapdh*_Fwd | CCATCACCATCTTCCAGGAGCGAG |
| *Gapdh*_Rev | GATGGCATGGACTGTGGTCATGAG |

(*Continued on next page*)

*Continued*

| Primer Name | Sequence |
|---|---|
| *Hsp90ab1*_Fwd | GCATGAAGGAGACCCAGAAG |
| *Hsp90ab1*_Rev | CACTGAGACCAGGCTCTTCC |
| *Hspa8*_Fwd | ATGTTGCTTTCACGGACACA |
| *Hspa8*_Rev | GGGCCAGTGCTTCATATCAG |
| *Ilf2*_Fwd | GCTCTTCTGATGCTACGGTGA |
| *Ilf2*_Rev | GAGAAGCGTTCTCTTCAAACC |
| *Kcnq2*_Fwd | TACCGCAAGCTGCAGAATTT |
| *Kcnq2*_Rev | CCCCTCAGAGCTCTTCTCGT |
| *Kcnq3*_Fwd | TGCCTGGTACATAGGCTTCC |
| *Kcnq3*_Rev | AGACGTCCTTCCCAGGTTTT |
| *Mog*_Fwd | GCAGGTCTCTGTAGGCCTTG |
| Mog_Rev | GTGCAGCCAGTTGTAGCAGA |
| *Ndufa4*_Fwd | AGGAGGTCCTGGGTGACTTT |
| *Ndufa4*_Rev | CAGTACCCCCTGCTCCAATA |
| *Neurod6*_Fwd | TGGAAAGGGTCAAGTTCAGG |
| *Neurod6*_Rev | GGTCTCTTGCCAATCCTCAG |
| *Rpl13*_Fwd | CACTCTGGAGGAGAAACGGAAGG |
| *Rpl13*_Rev | GCAGGCATGAGGCAAACAGTC |
| *Slc17a7*_Fwd | CTGGGGTCCTTGTGCAGTAT |
| *Slc17a7*_Rev | AACAGGGTTCATGAGCTTGG |
| *Slc32a1*_Fwd | CTGGAACGTGACAAATGCCA |
| *Slc32a1*_Rev | CGGCGAAGATGATGAGGAAC |
| *Snap25*_Fwd | AAAAAGCCTGGGGCAATAAT |
| *Snap25*_Rev | CTCACCTGCTCCAGGTTCTC |
| *TdTomato*_Fwd | GGCATTAAAGCAGCGTATCC |
| *TdTomato*_Rev | CTGTTCCTGTACGGCATGG |

## Primary cell culture

Primary hippocampal neurons were generated from E16.5 embryos using a standard protocol (Schraut et al., 2021). Briefly, dissected hippocampi were harvested in ice-cold dissection medium (HBSS, 7 mM HEPES, 2 mM L-glutamine, 500 U/mL penicillin-streptomycin, all Thermo Fisher Scientific). The tissue was incubated for 10 min in 0.25% trypsin-EDTA with 8 mM HEPES (Thermo Fisher Scientific) in a water bath at 37°C. Tissue was washed three times with serum medium (DMEM, 10% FBS, Thermo Fisher Scientific). The cells were dissociated by titration using glass Pasteur pipets in serum medium and filtered with a 70-μm cell strainer (Corning). Cell culture plates were coated overnight with 0.05 mg/mL poly-D-lysine mol wt 70,000–150,000 (Sigma Aldrich) in 0.15 M borate buffer (pH = 8.5). Cells were seeded in 24-well plates at a density of $5 \times 10^4$ cells in 1-mL growth medium (Neurobasal A medium, 1× B27 supplement, 0.25 × GlutaMAX, all Thermo Fisher Scientific) per well. All cultures were kept in a humidified incubator at 37°C and 5% $CO_2$. Growth medium was renewed after 7 days of culture. For all experiments, mature twenty-one-day-old primary neuronal cultures were used.

## *Ex vivo* electrophysiological recordings

### *Animals*

CD-1 (ICR) male mice (5-weeks-old) were purchased from Harlan Laboratories (Jerusalem, Israel). Mice were kept in groups of 4 or 5 animals per cage and were 7- to 8-week-old at the beginning of the experiment. Throughout the experiments, the animals were maintained in a temperature-controlled room (22°C ± 1°C) and constant humidity (55% ± 10%) on a 12-h light-dark cycle (lights on at 7 a.m.). Food and water were given *ad libitum*. All experimental protocols were approved by the Institutional Animal Care and Use Committee of the Weizmann Institute of Science. One week before the start of the experiment, the animals were single-housed and randomly assigned to the vehicle- or ketamine-treated group. Mice were handled following the same protocol used for the scRNA-seq experiments. Each animal received an intraperitoneal injection of 10 mg/kg/BW ketamine (or saline- for vehicle-treated mice) 30 min before being subjected to a 6-min FST (*see description of the FST above*). Mice were then returned to their home cage and left undisturbed for 36 h before being used for electrophysiological recordings.

### *Brain slices preparation*

All Mice were injected with pentobarbital (100 mg/kg i.p.) and perfused with carbogenated (95% $O_2$, 5% $CO_2$) ice-cold slicing solution containing (in mM): 2.5 KCl, 11 glucose, 234 sucrose, 26 $NaHCO_3$, 1.25 $NaH_2PO_4$, 10 $MgSO_4$, 2 $CaCl_2$; pH 7.4, 340 mOsm. After decapitation, 300-μm-thick horizontal slices containing the vHipp were prepared in carbogenated ice-cold slicing solution using a vibratome (Leica VT 1200S) and allowed to recover for 20 min at 33°C in carbogenated high osmolarity artificial cerebrospinal fluid (aCSF) (high-Osm) containing: 3.2 mM KCl, 11.8 mM glucose, 132 mM NaCl, 27.9 mM $NaHCO_3$, 1.34 mM $NaH_2PO_4$, 1.07 mM $MgCl_2$, 2.14 mM $CaCl_2$; pH 7.4, 320 mOsm. Subsequently, slices were incubated for 40 min at 33°C in carbogenated aCSF containing: 3 mM KCl, 11 mM glucose, 123 mM NaCl, 26 mM $NaHCO_3$, 1.25 mM $NaH_2PO_4$, 1 mM $MgCl_2$, 2 mM $CaCl_2$; pH 7.4, 300 mOsm. Finally, slices were kept at room temperature (23°C–25°C) in the same solution until use.

### *In vitro* electrophysiological recordings

Primary hippocampal neurons were generated from E16.5 embryos and cultured for 21 days, as described above (*see Primary Cell Culture*). Somatic whole-cell voltage-clamp recordings (>1 GΩ seal resistance, <20 MΩ series resistance, −70 mV holding potential, 2-kHz low-pass filter, 6 kHz sampling rate, 10 mV liquid junction potential correction) in saline or HNK (10 μM, 24 h)-treated cultures were performed at 25°C using an EPC9 amplifier. Cells were superfused (2–3 mL/min) with carbogenated aCSF containing: 125 mM NaCl, 2.5 mM KCl, 25 mM $NaHCO_3$, 1.25 mM $NaH_2PO_4$, 2 mM $CaCl_2$, 1 mM $MgCl_2$, 10 mM D-glucose, 5 mM 4-aminopyridine, 0.001 TTX, and 0.02 ZD7288. Patch pipette solution consisted of: 130 mM K-gluconate, 5 mM NaCl, 2 mM $MgCl_2$, 0.5 mM EGTA, 10 mM HEPES, 2 mM Mg-ATP, 0.3 mM Na-GTP, 20 mM phosphocreatine, and 5 D-glucose. M-current measurements/analyses were conducted as described for slice recordings (*see above*).

### Cloning and validation of shRNA constructs

The control shRNA scramble and Kcnq2 shRNA1 sequences were previously described (Valdor et al., 2018). The Kcnq2 shRNA2 sequence was designed using siRNA wizard software (Invitrogen). The shRNA sequences were synthesized in the pcDNA3 expression vector with the KpnI and BamHI restriction sites flanking the shRNA sequence (BioCat).

***Control shRNA:***

ggtacc***GATCCCACTACCGTTGTTATAGGTGTTCAAGAGACACCTATAACAACGGTAGTTTTTTTG***ggatcc

**Kcnq2 *shRNA1:***

ggtacc***GATCCCGGTATTCGGTGTTGAGTACTTCAAGAGAGTACTCAACACCGAATACCTTTTTTG***ggatcc

**Kcnq2 *shRNA2:***

ggtacc***GATCCCCGTGGTATTCGGTGTTGAGTACCAAGAGGTACTCAACACCGAATACCACGTTTTTTG***ggatcc

A pAAV-H1-EF1a-eGFP backbone was linearized using KpnI and BamHI restriction enzymes, opening up a region right after the H1 promoter. The shRNA fragments were digested with KpnI and BamHI and ligated into the pAAV-H1-EF1a-eGFP backbone using T4 DNA ligase according to the provided protocol (NEB). This generated the following three vectors, pAAV-H1-Ctrl-shRNA-EF1a-eGFP, pAAV-H1-KCNQ-shRNA1-EF1a-eGFP, and pAAV-H1-KCNQ-shRNA2-EF1a-eGFP. All plasmids were checked for mutations by DNA sequencing. The constructs were validated in mouse neuroblastoma N2a cells. These cells were maintained at 37°C with 5% CO2 in Minimum Essential Medium (MEM), 1× GlutaMAX, supplemented with 1× nonessential amino acids, 1 mM sodium pyruvate, 100 U/mL penicillin, 100 μg/mL streptomycin and 10% FBS (Thermo Fisher Scientific). Cells were detached with trypsin and transfected using ScreenfectA (ScreenFect GmbH) according to the manufacturer's protocol and maintained for two days before analysis. For imaging, cells were fixed with 4% PFA-PBS solution and embedded with Fluoromount-G mounting medium containing DAPI (Southern Biotech). Cells were imaged using an Axioplan 2 fluorescent microscope (Zeiss). For qPCR analysis, RNA was extracted and *Kcnq2* expression was determined using qPCR (see reverse transcription and qPCR methods section).

### Virus production and stereotactic surgery

The production of rAAV particles was previously described (Fiori et al., 2021). The rAAVs were produced with capsids of serotypes 1/2. The number of viral genomic particles was determined using qPCR resulting in titers of 2–5 × $10^{12}$ gp/mL. For viral injections, CD-1 mice were anesthetized with isoflurane and placed on a 37°C heating pad in a stereotactic apparatus (TSE Systems). Pre-surgery, mice were given Novalgin (200-mg/kg body weight) and Metacam (sub-cutaneous 0.5-mg/kg body weight). During surgery, mice were continuously supplied with 2% v/v isoflurane in $0_2$ through inhalation. AAV was injected bilateral using a 33-gauge injection needle with a 5 μL Hamilton syringe coupled to an automated microinjection pump (World Precision Instruments). For molecular studies 0.5 μL virus was injected at a rate of 0.1 μL/min. The injection coordinates were determined using the Franklin and Paxinos mouse brain atlas, from bregma: ML +/−3.2 mm bilateral; AP −3.2 mm; DV 3.5 mm. After injection the needle was retracted 0.01 mm and kept at the injection site for 1 min/0.1 μl of injected volume, followed by slow withdrawal. After surgery, the animals received Metacam for at least three days (intraperitoneal 0.5-mg/kg body weight). After completion of the behavioral experiments the injection sites were verified based on eGFP expression. Brains were fixed overnight with 4% paraformaldehyde-PBS followed by dehydration in 30% sucrose-PBS solution for at least 24 h at 4°C. Brains were cut in 50-μm thick sections using a vibratome (HM 650 V, Thermo Scientific). Brain slices were embedded in DAPI containing Fluoromount-G mounting medium (Southern Biotech). Slices were imaged with a VS120-S6-W slide scanner microscope (Olympus) or with a LSM800 confocal microscope (Zeiss).

### Chronic social defeat stress paradigm

C57BL/6N and Nex-Cre-Ai9 males (7-weeks-old) were exposed to the CSDS paradigm for 10 consecutive days, as previously described (Lopez et al., 2021). Experimental mice were introduced daily into the home cage of a dominant CD1 resident mouse, which rapidly recognized and attacked the intruders. To avoid serious injuries, the subordinate mouse was separated immediately after being attacked by the CD1 aggressor. After the physical encounter, mice were separated by a perforated metal partition, allowing the mice to keep continuous sensory but not physical contact for the next 24 h. Every day, for a total of 10 days, mice were defeated by another unfamiliar, CD1 mouse, to exclude a repeated encounter throughout the experiment. Defeat encounters were randomized, with variations in starting time (between 8:00 a.m. and 6:00 p.m.) to decrease the predictability to the stressor and minimize habituation effects. Control mice were single-housed, in the same room as the stressed mice, throughout the course of the experiment. All animals were handled daily and weighed every 2–3 days. Coat state was scored on a scale of 0 to 3 according to the following criteria: (0) No wounds, well-groomed and bright coat, and clean eyes; (1) no wounds, less groomed and shiny coat, OR unclean eyes; (2) small wounds, AND/OR dull and dirty coat, and not clear eyes; (3) extensive wounds, OR broad piloerection, alopecia, or crusted eyes. End point and tissue collection were performed in the morning (8:00 a.m.) and 24 h after the last social defeat session (day 11). This was done to capture the cumulative effects of chronic stress, rather than the acute effects of the last defeat session. For end point, all mice were deeply anesthetized with isoflurane and target tissues were quickly dissected for molecular experiments. Cardiac blood was collected for the assessment of basal CORT levels. Adrenal glands were dissected from fat and weighed. The brains were collected for dissection of the vHipp.

### Home cage activity

The home cage activity was measured with the Mouse-E-Motion infrared-detecting devices (infra-e-motion, Germany). Mice were single housed in fresh cages, and a metal food tray was employed to hold the devices in place. The base bedding was kept, but extra nesting materials that could conceal the animal were removed. The readout lasted 2 days (postinjection) during which time the animals were not disturbed. Locomotor activity was detected in 5-min increments and averaged by the hour. The final analysis was applied to the first 60-min period and the 48 h (2 days), postinjection.

### Plasma CORT measurements

Blood sampling was performed during end point (8:00 a.m.) by collecting trunk blood after decapitation. All blood samples were kept on ice and centrifuged at 4°C, and 10 μL of plasma was removed for measurement of CORT. All plasma samples were stored at −20°C until CORT measurement. CORT concentrations were quantified by radioimmunoassay (RIA) using a CORT double antibody 125I RIA kit (sensitivity: 25 ng/mL; MP Biomedicals Inc.) following the manufacturer's instructions. Radioactivity of the pellet was measured with a gamma counter (Wizard2 2470 Automatic gamma Counter; PerkinElmer). All samples were measured in duplicate, and the intra- and inter-assay coefficients of variation were both below 10%. Final CORT levels were derived from the standard curve.

### Pharmacological experiments

#### In vitro *treatments*

Primary hippocampal neurons were generated from E16.5 embryos and cultured for 21 days, as described above (see Primary Cell Culture). Because it is still not clear if primary neurons can metabolize (*R*,*S*)-ketamine in the same way that living mice can after i.p. treatment (Zanos et al., 2016), we performed these experiments using both ketamine and its active metabolite, (2*R*,6*R*)-HNK. For experiment 1 (Figure 3), neurons were treated with a saline solution, ketamine (10 μM), or (2*R*,6*R*)-HNK (10 μM) (Sigma, Cat #SML1873-25MG) for 0, 2, 12, 24 or 48 h and compared to untreated controls. For experiment 2 (Figure 6), neurons were stimulated with either a saline solution, (2*R*,6*R*)-HNK (10 μM), or a combination of (2*R*,6*R*)-HNK (10 μM) plus nifedipine (10 μM) (Tocris Bioscience, Cat # 1075), W-7 hydrochloride (10 μM) (Tocris, Cat #0369), or cyclosporine-A (1 μM) (Tocris, Cat #1101) for 30 min, 1, 2, or 6 h, and compared to untreated controls.

#### In vivo *treatments*

C57BL/6N and CD-1 (ICR) male mice aged 10 weeks old were used for these experiments. Ketamine hydrochloride (Ketaset, Zoetis, Germany) was diluted in 0.9% NaCl solution (saline) and administered i.p. at 1, 5 or 10 mg/kg/BW, depending on the experiment design. The KCNQ inhibitor, XE991 (Alomone Labs, Jerusalem, Israel; Cat #: X-100) was diluted in 5% DMSO and administered i.p. at 1 or 3 mg/kg/BW. The KCNQ activator, retigabine, also known as ezogabine (Alomone Labs; Cat#: R-100), was diluted in 5% DMSO and administered i.p. at 1 or 5 mg/kg. As control, mice were injected with a DMSO-saline solution (5% DMSO). For all experiments, mice were tested 30 min after injection in the FST.

### The social box arenas

The behavior of mice was studied in specialized "Social Box" (SB) arenas, designed for automated tracking of individual and group behaviors, as described previously (Anpilov et al., 2020; Forkosh et al., 2019; Karamihalev et al., 2020). Each arena housed four male mice that had been grouped together at the time of weaning. The SB consisted of an open 60 × 60 cm box and included the following objects: a covered nest, an open small nest, an S-shaped wall, two water bottles, two feeders and two elevated ramps. Food and water were available *ad libitum*. The arenas were illuminated at ca. 2 lx during the dark phase (12 h) and at ca. 200 lx (using light-emitting diodes) during the light phase (12 h). The fur of all mice was painted using four different hair dyes under mild isoflurane anesthesia.

The period under anesthesia was typically no longer than 10 min and the mice were left to recover for several days before the start of the experiment. A color-sensitive camera (Manta G-235C, Allied-Vision) was placed 1 m above the arena and recorded the mice during the dark phase. Mouse trajectories were automatically tracked offline using a combination of both a specially written software in MATLAB (MathWorks, Natick, MA, United States of America) Shemesh et al., 2013, 2020, and the markerless pose estimation software DeepLabCut (DLC, v. 2.1.10) (Mathis et al., 2018). On day 1, animals were transferred to the SB, for a total of 4 days of baseline (four dark and three light periods). On day 5, mice were removed from the SB and were administered either ketamine (10mg/kg BW) or saline intraperitoneally, followed by a FST 30 min later. All mice were subsequently returned into a clean SB for response monitoring over the following 36 h (2 dark and 1 light period). Normalized SB behavioral readouts (a total of 306 features) were summarized in 3 h time bins for the Baseline and Response days (days 3–6). To account for baseline individual differences, we calculated the change in each readout for each time bin from the mean of the corresponding time bin over the Baseline days. The change values from the first 3-h period of day 5 (immediately following the injection and FST procedure) were used to train a supervised partial least squares-based classifier.

### Characterization of the mouse behavioral response to ketamine

To gage the acute effects of pharmaceutical manipulations, we limited the analysis of the SB tracks to the first 3 h of the dark phase (immediately following the FST, *details below*). Likewise, the tracks from the Baseline days 3 and 4 were limited to the corresponding segment of the dark phase. DLC was used to track three key points (the nose, the center of mass, and base of the tail) for each individual for the duration of these videos. Preprocessing of the trajectory data and summaries of behavioral readouts were performed using a set of custom R functions. We extracted 306 behavioral readouts (features) for each individual in each of three separate dark phases. The median of each feature over the two Baseline days was used to create a baseline assessment. We transformed each feature within each stage/cohort combination to approximate a Gaussian distribution using a rank-based inverse normal transformation (Blom transform, *rankNorm* function in the *RNOmni* R package, v.1.0) (Z. 2019). The transformed values were used to calculate individual change scores (Response – baseline) for each feature. The ketamine response score was developed using PLS-DA, as implemented in the *mixOmics* package in R (v. 6.12.2) (Rohart et al., 2017). The training dataset consisted of 64 individuals (48 received ketamine (10 mg/kg/BW) and 16 received saline) and the input data consisted of the SB behavioral change scores combined with all FST behavioral readouts.

## QUANTIFICATION AND STATISTICAL ANALYSIS

All graphs represent mean ± SEM. All graphs show individual data points throughout the paper. For each graph, the sample size and statistical test used are described in the corresponding figure legend. No method was used to predetermine whether the data met assumptions of the statistical approach. For mouse experiments n is the number of mice whereas for *in vitro* experiments n is the number of cells. For all *in vitro* experiments, both the number of cells and biological replicates is specified.

### scRNA-seq

#### *Pre-processing, quality control and normalization*

For the initial quality check, *FastQC* (Simon, 2019) was employed before demultiplexing the cells by bar code using *Jemultiplexer* version 1.0.6 (Girardot et al., 2016) requiring a perfect match of the sequence. Adaptor trimming was performed using *cutadapt* version 1.11 (Martin, 2011). To extract and collapse unique molecular identifiers (UMIs) from the sequencing data, *UMI-tools* version 0.5.4 (Smith et al., 2017) modules extract and *dedup* (deduplication mode per gene) were used. Alignment and subsequent quantification after UMI deduplication were carried out by *Salmon* version 0.8.2 (Patro et al., 2017), specific settings included *noLengthCorrection*, *perTranscriptPrior* and *noEffectiveLengthCorrection* to accommodate tag sequencing. The mouse genome assembly (mm10) and corresponding gene annotation was used for alignment and quantification. As transcriptomic reference, known RefSeq transcripts with the addition of mitochondrial genes were used.

Data processing and analysis was done in *scanpy* (Wolf et al., 2018) (version 1.5.1) using AnnData as a data format (version 0.7.5). After considering the joint distribution of count depth, the number of genes expressed, and mitochondrial (MT) read fraction per sample, cells with more than 42,000 counts, with fewer than 700 genes expressed, and with 20% or more reads aligned to mitochondrial genes were filtered out. Furthermore, genes that were measured in fewer than 20 cells were also removed from the dataset. Quality control plots can be found in Figure S1A. This left a dataset of 5,013 cells and 20,670 genes. To assess which genes might be affected by ambient RNA signal, we computed the Gini coefficient per gene (https://github.com/oliviaguest/gini; retrieved Jan. 2021) and the zero-expression rate (also called dropout rate) per gene. The Gini coefficient assesses how evenly spread the expression of a gene is. We reason that potential ambient genes are those genes that have a lower dropout rate than would be expected given how evenly they are expressed. To quantify this, we fitted a linear model using numpy's *polyfit* function to predict dropout rate from the Gini coefficient. Potential ambient genes are defined as genes that have a lower actual dropout rate than predicted from the linear fit by a margin of over 1.5 times the standard deviation of the regression coefficient. This resulted in 9 potentially ambient genes (*Apoe*, *Hbb-bs*, *Trf*, *Ptgds*, *Hba-a2*, *Tcf4*, *Cst3*, *Plp1*, *Hba-a1*), which we ignored when assigning labels and did not consider in our differential expression evaluation.

Normalization and batch correction were performed in a two-stage process. First, size factors for each cell were computed using scran pooling (Lun et al., 2016) (scran R package, version 1.18.3). These size factors were used to normalize the data for the selection of highly variable genes. In a second step, the scran pooling size factors, a batch covariate, and the number of UMI per gene were used as a covariate in a negative binomial regression model fit to the count data following (Mayer et al., 2018). The Pearson residuals from this fit were used as a quantification of the expression values. Scran pooling was performed as implemented in the *computeSumFactors*() function. We passed a pre-clustering of the data to facilitate the fitting procedure (using log CPM+1, Euclidean distance on the top 50 PCs to construct a k-nearest neighbor graph with k = 15, and louvain clustering at resolution 1; see *clustering methods below*), and set the *min_mean* parameter to 0.1. In a second step, we fit a regularized negative binomial model to each gene as described in (Mayer et al., 2018). For each gene *i*, we fit the model:

$$log(E(Y_{ij})) = \beta_0 + \beta_1 B_j + \beta_2 U_j + \beta_3 S_j$$

Here $E(Y_{ij})$ denotes the expected value of the UMI count distribution of gene I across cells j, $B$j denotes the batch covariate of cell j, $U$j denotes the number of UMIs per expressed gene in cell j, and $S$j represents the scran pooling size factor for cell j. $\beta$ denotes a regression coefficient. The iCell8 chip identifier was used as a batch covariate. As proposed in the sctransform normalization paper (Hafemeister and Satija, 2019), this model was regularized by fitting a Poisson regression with the above model per gene to obtain an empirical dispersion parameter, $\theta$, then a regularized dispersion parameter was obtained by fitting a loess fit to the mean-variance relationship across genes. As we included the batch covariate in the above model, we could use the Pearson residuals of the regularized negative binomial regression as a batch-corrected expression unit for downstream analysis.

#### *Clustering, sub-clustering, marker gene detection, and cluster annotation*

We performed graph-based clustering on the computed KNN graph using the python implementation (version 0.6.1) of the Louvain algorithm in *Scanpy*. As a starting point, we performed a Louvain clustering at a resolution of 1. For each cluster, marker genes were determined by applying Welch's t test (as implemented in *Scanpy's rank_genes_groups* function with default parameters) between the cells in the cluster and all other cells. Differential expression testing for marker gene detection was performed on the log-scran normalized, non-batch-corrected expression values as recommended by published best practices (Luecken and Theis, 2019). We annotated clusters using a set of literature-derived markers (Zeisel et al., 2018). Marker-based annotation was performed by comparing the mean, scaled expression of all cells in a cluster, both on the level of individual markers and of marker sets associated with a cell identity label. Clusters that could not be distinctly annotated were merged (e.g., astrocyte subclusters, and glutamatergic neuronal subclusters), and further subclustering was performed at a louvain resolution of 0.4 to distinguish glutamatergic and GABAergic neurons, vascular cells from pericytes, and perivascular macrophages from microglia. Two populations without distinct marker gene signatures were removed as low quality cells. After discarding these populations, we were left with 13 annotated clusters.

#### *Differential expression analysis*

Differential expression analysis per cell identity cluster was performed via the limma package (version 3.46.0) (Ritchie et al., 2015). Specifically, we used the limma-trend pipeline, replacing CPM normalization with the scran pooling normalization we described above. For each annotated cluster, we fit the following linear model to all genes expressed in at least 10% of the cells in that cluster:

$$Y_{ij} \sim 1 + B_j + C_j$$

Here, $C_j$ represents the condition label (ketamine or saline) of cell j, $B_j$ represents the batch covariate label of the cell, and 1 denotes that an intercept was fit. The iCell8 chip identifier was used as batch covariate. This above model was fit using log-normalized data (from scran pooling normalization), and an empirical Bayes prior was used to fit the gene-wise variances via limma's *eBayes* function. DEGs were filtered out if expression was < 1 in both conditions. Multiple testing correction was performed using the Benjamini-Hochberg method.

### Reverse transcription and qRT-PCR

Real-time PCR reactions were run in triplicate using the ABI QuantStudio6 Flex Real-Time PCR System and data was collected using the QuantStudio Real-Time PCR software (Applied Biosystems). Expression levels were calculated using the standard curve, absolute quantification method. The geometric mean of the endogenous expressed genes *Rpl13* and *Gapdh* were used to normalize the data.

### *Ex Vivo* electrophysiological recordings

#### *Patch-clamp recordings and M-currents isolation*

CA1 pyramidal neurons were patched under visual guidance using infrared differential interference contrast (DIC) microscopy (BX51W1, Olympus) and an Andor Neo sCMOS camera (Oxford Instruments). Borosilicate glass pipettes (BF100-58-10, Sutter Instrument, Novato, CA, USA) with resistances 4–6 MΩ were pulled using a laser micropipette puller (P-2000, Sutter Instrument) and filled with intracellular solution: 135 mM potassium-gluconate, 4 mM KCl, 2 mM NaCl, 10 mM HEPES, 4 mM EGTA, 4 mM Mg-ATP, 0.3 Na2-GTP, 10 phosphocreatine-Na2, 280 mOsm, pH adjusted to 7.3 with KOH). Somatic whole-cell voltage-clamp recordings from CA1 pyramidal neurons (>1 GΩ seal resistance, −70 mV holding potential) were performed using a Multiclamp 700b.

amplifier (Molecular Devices). Data were acquired using pCLAMP 10.7 on a personal computer connected to the amplifier via a Digidata-1440 interface (sampling rate: 20 kHz; low-pass filter: 4 kHz), and analyzed with Clampfit 10.7 (all Molecular Devices). Data obtained with a series resistance > 20 MΩ were discarded.

All experiments were conducted at room temperature. In the recording chamber, slices were superfused with carbogenated aCSF (4–5 mL/min flow rate) containing 0.2 mM CdCl2, 1. μM TTX, 10. μM ZD7288, and 4 mM 4-aminopyridine, to block voltage-dependent Cav, Nav, HCN, and Kv1 channels, respectively. Synaptic activity was blocked with 10 μM NBQX-Na2 (2,3-dioxo-6-nitro-1,2,3,4-tetrahydrobenzo[f]quinoxaline-7-sulfonamide disodium salt), 50. μM D-APV (D-2-amino-5-phosphonopentanoic acid) and 10 μM (-)-bicuculline methiodide. To isolate M-currents, the following protocol was applied to the recorded cell, modified from Nigro et al. (2014): (1) a 1 s step from the holding potential (−70 mV) to −10 mV was applied (to activate IM while inactivating most other voltage-gated currents), (2) a 1 s step to −50 mV (to elicit IM tail current), and (3) a 0.5 s step to −10 mV, before returning to the holding potential. This procedure was repeated every 10 s for 5 min as baseline.

To investigate the effect of ketamine treatment on KCNQ2/3, the selective KCNQ2/3 inhibitor, XE991 (40 μM), was then bath applied and its effects were measured on the fast component of the tail current ($I_{tail}$), after 10 min of application. The $I_M$ tail current was measured by digitally subtracting the current obtained in XE991 condition to the current obtained in baseline condition. NBQX, D-APV, TTX-citrate, (−)-bicuculline methiodide, 4-aminopyridine, XE991 [10,10-bis(4-pirinydilmethyl)-9(10H)-antracenone] were obtained from Alomone Labs, and ZD7288 from Tocris Bioscience. All the remaining chemicals were obtained from Sigma-Aldrich.

### The social box arenas

Mouse trajectories were automatically tracked offline using a combination of both a specially written software in Matlab (Mathworks, Natick, MA, United States of America) (Shemesh, 2020; Shemesh et al., 2013), and the markerless pose estimation software DeepLabCut (DLC, v. 2.1.10) (Mathis et al., 2018). Preprocessing of the trajectory data and summaries of behavioral readouts were performed using a set of custom R functions. We extracted 306 behavioral readouts (features) for each individual in each of three separate dark phases. The median of each feature over the two Baseline days was used to create a baseline assessment. We transformed each feature within each stage/cohort combination to approximate a Gaussian distribution using a rank-based inverse normal transformation (Blom transform, *rankNorm* function in the *RNOmni* R package, v.1.0) (Z. 2019). The transformed values were used to calculate individual change scores (Response – Baseline) for each feature. The ketamine response score was developed using PLS-DA, as implemented in the *mixOmics* package in R (v. 6.12.2) (Rohart et al., 2017). The training dataset consisted of 64 individuals (48 received ketamine (10 mg/kg/BW) and 16 received saline) and the input data consisted of the SB behavioral change scores combined with all FST behavioral readouts.